Redox Biology 69 (2024) 102990

Contents lists available at ScienceDirect

Redox Biology

journal homepage: www.elsevier.com/locate/redox

Lead aggravates Alzheimer's disease pathology via mitochondrial copper accumulation regulated by COX17

Dingbang Huang [a,1], Lixuan Chen [a,1], Qiuyi Ji [a], Yang Xiang [a], Qin Zhou [a], Kaiju Chen [a], Xiaoshun Zhang [a], Fei Zou [a], Xingmei Zhang [b], Zaihua Zhao [c], Tao Wang [c], Gang Zheng [c,**], Xiaojing Meng [a,*]

[a] Department of Occupational Health and Occupational Medicine, Guangdong Provincial Key Laboratory of Tropical Disease Research, School of Public Health, Southern Medical University, Guangzhou, 510515, China
[b] Department of Neurobiology, School of Basic Medical Sciences, Southern Medical University, Guangzhou, 510515, China
[c] Department of Occupational and Environmental Health and the Ministry of Education's Key Laboratory of Hazard Assessment and Control in Special Operational Environment, School of Military Preventive Medicine, Fourth Military Medical University, Xi'an, 710032, China

ARTICLE INFO

Keywords:
Pb
Microglia
Alzheimer's disease
Mitochondrial copper
Mitochondrial ROS

ABSTRACT

Alzheimer's disease (AD) is a common neurodegenerative disease that is associated with multiple environmental risk factors, including heavy metals. Lead (Pb) is a heavy metal contaminant, which is closely related to the incidence of AD. However, the research on the role of microglia in Pb-induced AD-like pathology is limited. To determine the mechanism by which Pb exposure aggravates AD progression and the role of microglial activation, we exposed APP/PS1 mice and $A\beta_{1-42}$-treated BV-2 cells to Pb. Our results suggested that chronic Pb exposure exacerbated learning and memory impairments in APP/PS1 mice. Pb exposure increased the activation of microglia in the hippocampus of APP/PS1 mice, which was associated with increased deposition of $A\beta_{1-42}$, and induced hippocampal neuron damage. Pb exposure upregulated copper transporter 1 (CTR1) and downregulated copper P-type ATPase transporter (ATP7A) in the hippocampus of APP/PS1 mice and $A\beta_{1-42}$-treated BV-2 cells. Moreover, Pb enhanced mitochondrial translocation of the mitochondrial copper transporter COX17, leading to an increase in mitochondrial copper concentration and mitochondrial damage. This could be reversed by copper-chelating agents or by inhibiting the mitochondrial translocation of COX17. The increased mitochondrial copper concentration caused by increased mitochondrial translocation of COX17 after Pb exposure may be related to the enhanced mitochondrial import pathway of AIF/CHCHD4. These results indicate that Pb induces the activation of microglia by increasing the concentration of copper in the mitochondria of microglia, and microglia release inflammatory factors to promote neuroinflammation, thus aggravating the pathology of AD. The present study provides new ideas for the prevention of Pb-induced AD.

1. Introduction

Lead (Pb) is a common heavy metal contaminant in occupational and living environments. It is highly neurotoxic and can damage the blood–brain barrier [1]. In the past decades, large amounts of Pb have been discharged into the air, water, and soil in different forms, posing a great threat to public health [2–4]. There is no established safe threshold for blood Pb levels, and even low levels of Pb in the blood can have negative impacts on human health [5]. The detrimental effects of Pb on the central nervous system (CNS) have been extensively studied and confirmed [6]. The damage to the CNS caused by Pb is primarily characterized by a decline in learning and memory abilities. This damage is directly linked to neuronal damage and neuroinflammation caused by Pb exposure [7,8] and may lead to Alzheimer's disease (AD),

* Corresponding author. Department of Occupational Health and Occupational Medicine, School of Public Health, Southern Medical University, 1838 Guangzhoudadaobei, Guangzhou, 510515, China.
** Corresponding author. Department of Occupational and Environmental Health, School of Military Preventive Medicine, Fourth Military Medical University, 169 Changlexi Road, Xi'an 710032, China.
E-mail addresses: zhenggang@fmmu.edu.cn (G. Zheng), xiaojingmeng@smu.edu.cn (X. Meng).
[1] These authors contributed equally to this work.

https://doi.org/10.1016/j.redox.2023.102990
Received 14 September 2023; Received in revised form 3 November 2023; Accepted 6 December 2023
Available online 9 December 2023

Parkinson's disease, and other neurodegenerative diseases [9,10].

AD is a neurodegenerative disorder that currently affects over 40 million people worldwide [11]. The main symptoms of AD include learning and memory impairment, as well as damage to the hippocampal region of the brain [12,13]. Recent studies suggest that neuroinflammation plays a significant role in AD pathogenesis [14–16]. Neuroinflammatory symptoms are often observed in patients with AD, and the continuous stimulation of microglia by Aβ and neuron fragments leads to the release of pro-inflammatory factors, which may cause chronic, irreversible inflammation and neuron damage [17].

Microglia, the resident immune cells of the CNS, produce inflammatory factors when stimulated by external factors [18]. Exposure to Pb has been found to affect gene expression in the hippocampus of mice, with microglia being the most vulnerable to its impact [19]. Additionally, Pb exposure can activate microglia to produce pro-inflammatory factors, leading to neuroinflammation [20]. The overproduction of inflammatory cytokines by activated microglia can damage neurons [21]. Research has indicated that Pb may contribute to the development of AD through inducing neuronal damage and activating astrocytes [22,23]. However, the role of microglia in this process remains uncertain.

One mechanism of Pb neurotoxicity is the disruption of cellular homeostasis of trace elements, including copper, calcium, and zinc. This disruption leads to abnormal physiological activities [24–26]. Studies have shown that Pb exposure can lead to an increase in copper concentration in the rat hippocampus [27,28]. Additionally, it was observed that Pb exposure can upregulate copper transporter 1 (CTR1) and downregulate copper P-type ATPase transporter 7A (ATP7A) in choroidal epithelial cells, resulting in an increase in intracellular copper ion concentrations [29]. Copper is an essential metal element and plays a crucial role in the activities of many enzymes that control a wide range of cellular biochemical and regulatory functions [30]. A recent study has shown that copper exposure in mice can cause oxidative stress, activate the NF-κB pathway, and lead to microglial activation [31]. Copper is known to play a role in AD by causing oxidative stress and promotes hyperphosphorylation of tau and aggregation of Aβ [32,33]. Recent clinical studies have revealed a prevalent copper imbalance among patients with AD. It has been observed that AD patients exhibit higher serum copper levels compared to healthy individuals [34,35]. Non-ceruloplasmim copper can have predictive value in conversion to full AD in patients with mild cognitive impairment [36]. Additionally, there is evidence suggesting a correlation between variations in the copper transporter gene and the development of AD. Notably, carriers of the ATP7B AG haplotype were found to be significantly more prevalent in the AD group, all of whom exhibited copper imbalances [37,38]. Mitochondria are one of the main sites for intracellular copper utilization. Cytochrome *c* oxidase assembly homolog 17 (COX17) is responsible for transporting copper ions from the cytoplasm to the mitochondrial respiratory chain complex [39]. In the case of excessive intracellular copper levels, copper will be transported to the mitochondrial matrix compartment for storage to prevent the occurrence of copper overload [40], which may also cause damage to the mitochondria. Further studies are required to investigate whether Pb-induced microglial activation is caused by mitochondrial damage due to cytoplasmic copper and mitochondrial copper turnover in the development of AD.

In the present study, we investigated (i) the impact of chronic Pb exposure on hippocampal and mitochondrial copper levels in APP/PS1 mice and (ii) how this affects microglia and nerve damage related to AD. We also examined the production of mitochondrial reactive oxygen species (mtROS) and the changes in the localization of COX17, which is involved in mitochondrial copper transport. To the best of our knowledge, this is the first study to identify the role of mitochondrial copper in Pb-induced microglial activation in animal and cell models of AD. Our study elucidates the molecular mechanism underlying the exacerbation of AD by Pb exposure and highlights the significant involvement of mitochondrial copper ion disruption in this process.

2. Materials and methods

2.1. Chemicals and antibodies

Lead acetate (PbAC) was purchased from Sigma (Darmstadt, Germany). $A\beta_{1\text{-}42}$ was obtained from the Chinese Peptide (Hangzhou, China). Bovine serum albumin (BSA) was obtained from ABCone (Shanghai, China). Anti-CTR1 and anti-ATP7A were purchased from Abcam (Cambridge, UK). Anti-IBA-1 and anti-iNOS were purchased from Cell Signaling Technology (CST) (Danvers, MA, USA). Anti-Aβ was obtained from CST (Danvers, USA). Anti-SCO1 was purchased from Santa Cruz Biotechnology (Dallas, USA). Anti-COX17, anti-SCO2, anti-COX16, anti-PAM16, anti-TOM20, anti-TOMM40, anti-CHCHD4, anti-ALR, and anti-TIM23 were purchased from Proteintech (Chicago, USA). The copper-chelating agent tetrathiomolybdate (TM) was purchased from Aladdin (Shanghai, China). JC-1 was purchased from ThermoFisher (MA, USA). CCK-8 proliferation detection kits were purchased from Dojindo (Tokyo, Japan). TNF-α and IL-6 ELISA kits were purchased from Beyotime (Shanghai, China).

2.2. Animals and treatments

All animal experiments were approved by the Animal Ethics Committee of Southern Medical University (Approval No. L2021042) and complied with the guidelines issued by Southern Medical University for the Care and Use of Laboratory Animals. Three-month-old female C57BL/6J mice were purchased from the Experimental Animal Center of Southern Medical University, and male APP/PS1 double transgenic mice were purchased from Beijing HFK Bio-Technology Co. Males and females were mated at a ratio of 1:3. Females were examined daily for vaginal plugs to determine pregnancy dates. All pups were labeled by stud earring, and then, the pups with the same genotype were pooled. Twenty (female, $n = 10$; male, $n = 10$) 3-week-old APP/PS1 double transgenic mice and 24 (female, $n = 12$; male, $n = 12$) 3-week-old C57BL/6 mice were randomly divided into four groups according to genotype and gender (WT group, female, $n = 6$; male, $n = 6$; WT + Pb group, female, $n = 6$; male, $n = 6$; APP/PS1 group, female, $n = 5$; male, $n = 5$; APP/PS1 + Pb group, female, $n = 5$; male, $n = 5$). The mice were continuously chronic exposed from 3 weeks to 4 months of age. Mice in the WT + Pb and APP/PS1 + Pb groups were exposed to Pb via drinking water (100 ppm PbAC), while mice in the WT and APP/PS1 groups were fed the same volume of normal saline. Body weight, food intake, and water intake were recorded weekly. After 4 months, the mice were subjected to a novel object recognition (NOR) test and a Morris water maze (MWM) test to assess their memory and learning abilities. At the end of the behavioral tests, all mice were euthanized. Blood and brain tissue were collected from each mouse for subsequent analysis (Fig. 1A).

2.3. Morris water maze test

Spatial memory formation and retention were evaluated using the MWM test. The pool was divided into four quadrants (Q1, Q2, Q3, and Q4) containing water with milk powder at a temperature of 22–24 °C. A hidden platform was placed 2–3 cm below the surface in Q4. The pool had a diameter of 1.3 m, and the platform had a diameter of 15 cm. A camera connected to a computer was used to track the movement of mice as they navigated toward the platform. The time taken for the mouse to find the platform (escape delay) and the distance it traveled were recorded. The experiments lasted for 6 days, with the first 5 days dedicated to positioning navigation. The escape incubation period was calculated as the time between entering the water and finding the platform, with each trial starting from a different quadrant of the pool. Mice that could not find the platform within 60 s were placed on the platform for 15 s. On the final day of the experiment, the platform was removed, and the mice were given 60 s to explore the pool. Swimming time, the total swimming distance in the platform quadrant, and the

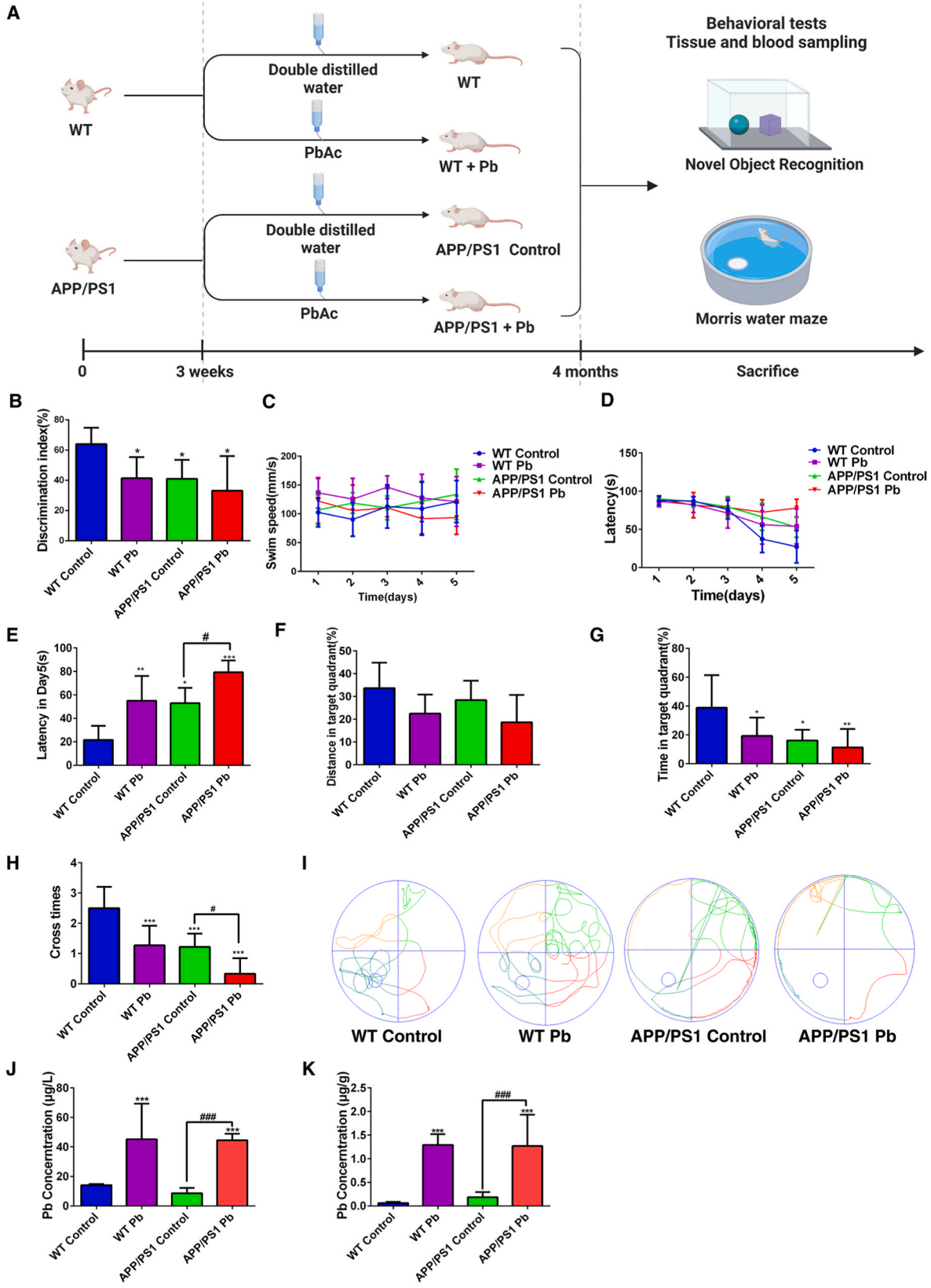

Fig. 1. Effects of Pb exposure on learning and memory in APP/PS1 mice. (A) Schematic workflow of the APP/PS1 mouse Pb exposure experiment. The entire period was 4 months. Mice received either double-distilled water or lead-containing water starting at 3 weeks of age. All mice were tested in behavioral experiments at 4 months of age. (B) New object recognition index (%). (C–I) Water maze experiment to detect (C) the swimming speed (mm/s) during the first 5 days, (D) latency (s) in the first 5 days, (E) latency (s) on the fifth day, (F) the motion distance ratio in the target quadrant, (G) the percentage of movement time in the target quadrant, (H) the number of platform crossings, and (I) representative swimming tracks of mice. (J) Blood Pb concentration (μg/L) in mice and (K) hippocampus lead concentration (μg/g) in mice were determined using ICP-MS. $^{*}P < 0.05$, $^{**}P < 0.01$, $^{***}P < 0.001$ vs. WT control group; $^{\#}P < 0.05$, $^{\#\#\#}P < 0.001$ vs. APP/PS1 control group. WT control, $n = 10$; WT Pb, $n = 10$; APP/PS1 control, $n = 7$, APP/PS1 Pb, $n = 6$.

number of times the mice crossed the platform were recorded.

2.4. Novel object recognition test

The mice were placed in the experimental room for at least 1 h before starting the Novel object recognition (NOR) test to adapt to the environment. The room was quiet, with a temperature of 25 °C, and strong light was avoided. Before each experiment, the room was cleaned using 50 % ethanol. The experiment was operated in three stages. First, in the acclimatization stage, the mice were gently placed into a specially designed 45 cm × 45 cm × 45 cm cubic test chamber with black acrylic plates and put back into the cage after 5 min of free movement. In the familiarization phase, two identical objects were placed on the same side of the test chamber. The objects were odorless and could not be easily moved, and the objects were placed approximately 10 cm from the walls of the chamber on both sides. The mice were observed exploring the objects for 5 min. Finally, in the test phase, one of the objects was replaced with a new object and the exploration time of each object was recorded for 5 min, where exploration was defined as the time when the mouse's nose was within 2 cm of the object, including nose sniffing, licking the object, and resting on the object with its front paws. The time when the mouse stayed next to the object to rest or lay on the object without moving was not counted. The discrimination index (DI) was calculated as follows: DI = time spent exploring new object/total exploration time × 100 %.

2.5. Cell culture and treatments

BV-2 microglial cells were provided by Shandong University, and HT-22 hippocampal neurons were obtained from ATCC (Manassas, USA). The cells were cultured in high-glucose DMEM supplemented with 10 % BSA at 37 °C in a humidified atmosphere containing 5 % CO_2. PbAC was prepared as a 10 mM stock solution in deionized water. After the cells were incubated for 24 h, they were pretreated with $A\beta_{1\text{-}42}$ (10 μM) for 1 h and then co-treated with PbAC (10 μM) for 12 h. Cell supernatants were collected for ELISA. Cells were collected for immunofluorescence analysis, and cellular proteins were extracted for Western blot. The mitochondrial oxidative phosphorylation level and membrane potential were measured using kits according to the manufacturer's instructions.

2.6. Transmission electron microscopy

The morphological changes of mitochondria in the hippocampal region of mice were observed using transmission electron microscopy (TEM) (JEM-1400, JEOL Ltd., Tokyo, Japan), focusing on the normality and size of intracellular mitochondria, vacuoles, and mitochondrial cristae structures.

2.7. Western blot analysis

Proteins were separated by SDS-PAGE and transferred onto a PVDF membrane (Merck Millipore, MA, USA). The membranes were incubated for 1 h at room temperature in blocking buffer, followed by overnight incubation at 4 °C in blocking buffer containing the primary antibody including anti-CTR1 and anti-ATP7A (1:1000, Abcam, Cambridge), anti-PRX-3 and anti-VDAC(1:1000, Santa Cruz Biotechnology, Dallas), anti-AIF(1:1000, CST, Danvers), or anti-COX17, anti-TOM20, anti-TOMM40, anti-TIM23, anti-PAM16, anti-CHCHD4 (1:1000, Proteintech, Chicago), anti-β-actin (1:10000, Proteintech, Chicago) anti-β-Tubulin(1:10000, Proteintech, Chicago) and anti-GFER(1:1000, Proteintech, Chicago). Then, the membrane was washed three times before incubation with the secondary antibody IRDye 800CW Goat anti-Rabbit IgG (H + L) or IRDye 680RD Goat anti-Mouse IgG (H + L)(1:10000, LI-COR Biosciences, Lincoln) for 1 h at room temperature. Protein bands were detected using an Odyssey Infrared Imaging System (LI-COR Biosciences, Lincoln, NE, USA).

2.8. Immunohistochemistry

As described previously, immunohistochemistry (IHC) was used to analyze the activation of microglia and the distribution of Aβ plaques in the hippocampus of APP/PS1 mice. Briefly, paraffin sections were deparaffinized in xylene, rehydrated through a graded alcohol series, and then treated in 0.1 M Tris-buffered saline (TBS, pH 7.4) containing 3 % hydrogen peroxide (H_2O_2) for 10 min. Subsequently, the sections were boiled in citric acid for 3 min, treated with 5 % BSA for 30 min, and then incubated overnight with rabbit anti-IBA-1 (CST; 1:800) and mouse anti-Aβ (CST; 1:800) at 4 °C. Biotinylated goat anti-rabbit and goat anti-mouse IgG (1:200) were used to incubate the sections for 1 h, followed by streptavidin peroxidase incubation for 1 h. Next, 0.025 % diaminobenzidine (DAB) was used to stain the sections for 1 min. The stained sections were dehydrated through a graded alcohol series, cleared in xylene, and covered with neutral balsam. All sections were examined with a light microscope (Olympus, Tokyo, Japan).

2.9. Nissl staining

Fresh brain tissues were fixed with 4 % paraformaldehyde for 48 h, followed by dehydration, embedding, dewaxing, and sectioning. Sections were rinsed using distilled water and then placed into a staining bucket containing Nissl staining solution at 55 °C for 20–30 min. After rinsing with distilled water, they were transparently dehydrated and sealed with neutral resin. Histopathological abnormalities were observed under a light microscope (Olympus, Tokyo, Japan), and the dark neuronal cells were counted with ImageJ software.

2.10. Mitochondrial oxidative phosphorylation levels

Mitochondrial oxidative phosphorylation levels were detected using a kit according to the manufacturer's protocol (Agilent, CA, USA). In brief, a series of oxidative phosphorylation and electron transport chain inhibitors were used to determine the mitochondrial oxidative phosphorylation level using a Seahorse XF Analyzer (Agilent, CA, USA). The basal respiratory oxygen consumption level of cells was first determined. Then, oligomycin was added to inhibit ATP synthase to detect the oxygen consumption due to proton leakage. Next, the uncoupling agent FCCP was added to maximize the electron transfer rate, and the maximum oxygen consumption rate (OCR) was determined. Finally, antiA/Rot was added to completely inhibit the electron transport chain, and the non-mitochondrial oxygen consumption level was detected.

2.11. Hematoxylin and eosin staining

Paraffin-embedded slices were placed at 60 °C for 1 h and dewaxed in xylene for 10 min, followed by treatment with 100 %, 95 %, and 90 % ethanol for 10 min each and staining with hematoxylin and eosin (HE). Finally, the slices were observed under a light microscope (Olympus, Tokyo, Japan).

2.12. Measurement of the mitochondrial membrane potential

The mitochondrial membrane potential (Δψm) was monitored using a mitochondrial membrane potential assay kit (Invitrogen, CA, USA) employing the lipophilic cationic probe JC-1. In vivo, after the mitochondria of animal hippocampal tissue were isolated, they were incubated with JC-1 dye for 30 min at 4 °C in the dark. A flow cytometer (BD, NJ, USA) was used to record fluorescence. For in vitro experiments, 2×10^5 BV-2 cells were seeded on a 35-mm confocal plate. After treatments, the cells were incubated with JC-1 for 20 min at 37 °C in the dark and washed twice with ice-cold JC-1 buffer solution. The images were recorded by a confocal laser scanning microscope (FV1000, Olympus,

Tokyo, Japan).

2.13. CCK-8 assay

A CCK-8 assay kit was used according to the manufacturer's protocol (DOJINDO, Kyushu, Japan). First, 3.5×10^3 BV-2 cells per well were seeded in a 96-well flat-bottom culture plate. After treatments, 20 μL of CCK-8 solution was added to each well, and the samples were incubated at 37 °C for 3 h. Absorbance was measured using a spectrophotometer (ThermoFisher, USA) at 450 nm.

2.14. ELISA

To determine cytokine levels, TNF-α and IL-6 in the cellular culture supernatants or the hippocampus tissue lysates were measured by using TNF-α and IL-6 ELISA kits, respectively, according to the manufacturer's protocol (Beyotime, Shanghai, China). Absorbance at 450 nm was measured by using a spectrophotometer (ThermoFisher, MA, USA).

2.15. Oxygen consumption rate determination

Oxygen consumption rate (OCR) was measured at 37 °C using an XFe96 Extracellular Flux analyzer (Agilent Technologies). After treatments, the culture medium was changed to XF base medium (containing 1 mM pyruvate, 2 mM glutamine, and 10 mM glucose), and cells were incubated at 37 °C in a CO_2-free atmosphere for 1 h before measurement. After detection of basal OCR, responses were evaluated after the application of oligomycin (1 μM, ATP synthase complex inhibitor), FCCP (300 nM, uncoupler), and the combination of antimycin (1 μM, complex III inhibitor) and rotenone (1 μM, complex I inhibitor). From these measurements, various parameters of mitochondrial function were determined. After completion of the assay, total protein was isolated from individual wells and quantified. Oxygen consumption in each well was normalized to the amount of protein.

2.16. Inductively coupled plasma mass spectrometry (ICP-MS)

For measurements of copper levels in the tissues, the brain tissues were added into the tubes containing 2 mL of 65 % concentrated nitric acid and 1 mL of 30 % hydrogen peroxide and put the tubes in the room temperature for 1 h. Then, the samples were digested at 110 °C in the digestion furnace for 6 h, and continue to be digested at 100 °C for an additional 6 h. After digestion, copper content was determined using inductively coupled plasma mass spectrometry (ICP-MS) (X Series 2; Thermo Fisher Scientific, Waltham, MA, USA). For measurements of mitochondrial copper levels in the cells, mitochondria were isolated from 1×10^8 cells using a kit according to the manufacturer's protocol (Beyotime, Shanghai, China). Cells were washed with cold PBS, digested in 0.25 % trypsin, and centrifuged at 200 *g* for 10 min. The cell precipitates were resuspended in cold PBS and centrifuged at 4 °C at 600 *g* for 5 min. Next, 1–2.5 mL of mitochondrial separation reagent was added, and suspended cells were placed in an ice bath for 10–15 min. The cell suspension was transferred to a dounce homogenizer, and cells were homogenized about 10–30 times. Samples were first centrifuged at 600 *g* for 10 min at 4 °C and then at 11,000 *g* for 10 min at 4 °C. The supernatant was removed and 200 μL mitochondrial storage solution was added to resuspend the precipitate. Purity was determined by the ratio of VDAC1/ACTIN protein levels measured by Western Blot. Next, 0.1 % nitric acid was added to a final volume of 10 mL. The copper levels were determined using ICP-MS.

2.17. Immunofluorescence

For analysis of hippocampal tissues, hippocampus slides were washed with PBS, incubated in PBS with 0.3 % Triton-X 100 for 30 min, blocked in 20 % goat serum, and incubated with rabbit anti-IBA-1 (1:800) and mouse anti-Aβ (1:800) at 4 °C overnight. Subsequently, the slides were washed, incubated for 1 h at room temperature with a fluorescent secondary antibody, and observed under a confocal laser scanning microscope (FV1000, Olympus, Tokyo, Japan).

For the cell line, 2×10^5 BV-2 cells were seeded on a 35-mm confocal plate. After treatments, the cells were washed three times with PBS and fixed in 4 % paraformaldehyde for 15 min at room temperature. Then, the cells were washed three times with PBS, incubated with ice-cold methanol for 10 min at −20 °C, and blocked in 5 % BSA for 30 min at room temperature. The cells were incubated overnight at 4 °C with the appropriate primary antibody (1:100) in 5 % BSA and with the secondary antibodies (Alexa Fluor® anti-mouse 594 and anti-rabbit 488) (Thermo Fisher) (1:500) in 5 % BSA for 60 min at room temperature. The images were recorded by a confocal laser scanning microscope (FV1000, Olympus, Japan).

2.18. Fluoro-Jade C labeling

Paraffin-embedded slices were deparaffinized and dehydrated by the method of Michele Longoni Calió using a kit following the manufacturer's instructions [41]. The slides were then immersed in a solution of 80 % alcohol and 1 % sodium hydroxide, followed by a 2-min immersion in 70 % alcohol and another 2-min immersion in distilled water. The slides were incubated in a 0.06 % potassium permanganate solution for 10 min, incubated in a 0.0004 % Fluoro-Jade C (FJC) labeling solution for 30 min, and rinsed three times with distilled water for 1 min each. The slides were observed under a confocal laser scanning microscope (FV1000, Olympus, Tokyo, Japan).

2.19. Truncated COX17 mutants

The truncated mutants of COX17 were designed according to the method of Andrew B. Maxfield [42]. To obtain the stable expression cell lines, we used commercially packaged lentiviral vectors (Tsingke Biotechnology Co., Beijing, China). Lentiviral infection was performed according to the manufacturer's instructions. Infected cells were incubated in 5 μg/mL puromycin to select stable expression cell lines. The stable expression cell lines were validated by Western blotting after isolation of mitochondrial protein.

2.20. Co-immunoprecipitation assay

Binding of the mitochondrial protein CHCHD4 to COX17 was determined using a co-immunoprecipitation assay. We added 1 μg protein A antibody to 1 mg protein and incubated samples with slow shaking at 4 °C for 2 h. Protein A/G agarose beads and buffer solution were added to a new clean centrifuge tube and centrifuged at 4 °C for 2 min at 1100 g. This step was performed five times. Then, the beads were added to the protein sample, which was mixed well and incubated at 4 °C with slow shaking for 1 h. After that, it was centrifuged at 4 °C at 1100 g for 5 min, and the supernatant was aspirated. The pellet was then washed three times with IP buffer by centrifugation at 1100*g* for 5 min. Finally, an equal volume of 2 × sample buffer was added to the sample, which was incubated at 95 °C for 10 min and centrifuged. The supernatant was analyzed by SDS-PAGE and Western blot.

2.21. Statistical analysis

Results are expressed as the mean ± standard deviation. Student's *t*-test was used to determine the statistical significance of differences between two groups. One-way ANOVA was used to determine the statistical significance of differences between three or more groups. To analyze MWM data, repeated measures ANOVA was conducted, followed by the Tukey post hoc test. If the data did not meet the ANOVA criteria, the Kruskal–Wallis test (nonparametric ANOVA) was applied, followed by pairwise comparisons using the Wilcoxon rank sum test

based on a *P*-value corrected by Holm–Bonferroni correction. $P < 0.05$ was considered significant.

3. Results

3.1. Pb exposure aggravates AD pathology in APP/PS1 mice

The main manifestation of AD is learning and memory impairment and hippocampal damage [12,13]. Therefore, we examined the learning and memory ability and hippocampal damage in mice exposed to Pb. Three-week-old APP/PS1 mice and C57BL/6 mice were selected for the experiment and exposed to 100 ppm Pb until the age of 4 months. Then, the learning and memory ability was tested (Fig. 1A). The weight of mice was recorded weekly and there was no significant difference between the groups (Fig. S1). First, the NOR test and the MWM test were used to determine differences in learning and memory ability in mice. All three experimental groups (WT Pb, APP/PS1 control, and APP/PS1 Pb) exhibited a significant reduction in NOR compared to the WT control group (Fig. 1B), which suggests that Pb exposure caused short-term memory impairment in the mice. The MWM test results showed that Pb had no effect on the swimming speed of mice in each group during the first 5 days of training, which proved that Pb treatment did not affect the physical ability of mice (Fig. 1C). During the training period, the WT control group showed a significant decrease in latency on the third day compared to the first day. However, the WT Pb group, APP/PS1 control group, and APP/PS1 Pb group showed a significant decrease in latency on the fourth day (Fig. 1D). On day 5, the APP/PS1 Pb group exhibited significantly longer latency than the APP/PS1 control group (Fig. 1E). On the sixth day of the experiment, there was no significant difference in the relative distance covered in the target quadrant between groups (Fig. 1F), but the percentage of time in the target quadrant and the number of platform crossings of each group were significantly decreased compared with the WT control group (Fig. 1G and H). There was a notable difference in the number of platform crossings between the APP/PS1 Pb group and the APP/PS1 control group. Specifically, compared with the APP/PS1 control group, the number of platform crossings in the APP/PS1 Pb group was significantly lower (Fig. 1H). These findings suggest that Pb exposure may have a negative impact on the learning and memory abilities of mice. In addition, compared with the WT control group, Pb exposure significantly increased the blood and hippocampal Pb concentrations in the WT Pb group and the APP/PS1 Pb group (Fig. 1J and K).

Dark neurons are a typical representative of neuronal morphological changes after various injuries [43], so we conducted HE staining and Nissl staining to detect the morphology and arrangement of neurons after Pb exposure. In comparison to the WT control group, the nerve cells in the CA1, CA3, and DG regions of the hippocampus in the other groups were less densely distributed. Additionally, a significant number of cells appeared to have shrunk, and the staining was notably darker (Fig. 2A). Compared with the WT control group, the number of neurons in the CA1, CA3, and DG regions in the other three groups was significantly reduced, and the number of dark neurons in the CA1, CA3, and DG regions was significantly increased (Fig. 2B–D). The number of neurons in the CA1 and DG regions of the APP/PS1 Pb group was significantly reduced compared with the APP/PS1 control group, while the number of dark neurons was significantly increased (Fig. 2B–D). Aβ deposition was significantly increased in the APP/PS1 Pb group compared with the APP/PS1 control group (Fig. 2E). The FJC staining results showed that the number of degenerative neurons was increased in the APP/PS1 Pb group compared with the APP/PS1 group, indicating that Pb exposure aggravated the pathological manifestations of AD in APP/PS1 mice (Fig. 2F).

3.2. AD neuronal injury aggravated by Pb is associated with activation of microglia and secretion of inflammatory cytokines

A previous study has shown that Pb can induce microglial activation [8]. To determine whether Pb can promote microglial activation in AD pathology and whether neuronal injury is related to microglial activation, we determined the levels of the inflammatory cytokines TNF-α and IL-6 in the hippocampus tissue and serum of mice exposed to Pb as well as in the supernatant of BV-2 cells treated with Pb and $A\beta_{1\text{-}42}$. The results showed that the levels of TNF-α and IL-6 in the hippocampal tissue and serum were increased after Pb exposure compared with the non-exposed group with the same genotype (Fig. 3A and B). The levels of TNF-α and IL-6 in the cell culture supernatant were also higher in the Aβ+Pb group (Fig. 3C). IHC results showed that the resting microglia of the control group were small and round, with delicate branching processes. The cell bodies of the WT Pb group, the APP/PS1 control group, and the APP/PS1 Pb group were larger and the protrusions were coarse, which indicated the activation of microglia. The morphological changes were most obvious in the APP/PS1 Pb group (Fig. 3D). The immunofluorescence results of IBA-1 and Aβ in the hippocampus of mice revealed distinct characteristics. In the WT control group, microglia were observed to be small and round in the resting state, with fine branching processes. However, in the WT Pb group and the APP/PS1 group, the cell bodies appeared enlarged, and the protrusions became coarse and activated. Notably, the APP/PS1 group exhibited more pronounced changes, with more Aβ precipitation around the cells compared to the APP/PS1 control group (Fig. 3E). In the in vitro experiments, BV-2 cells in the control group showed either no protuberances or short ones. Upon treatment with $A\beta_{1\text{-}42}$, some cells exhibited enlarged or elongated cell bodies, with the severity being more pronounced after treatment with Pb and $A\beta_{1\text{-}42}$ (Fig. 3F). The increase of Inducible nitric oxide synthase (iNOS) in immunofluorescence study can be considered as a marker of microglia activation [44]. iNOS expression was found to be low in the control group but was increased in the $A\beta_{1\text{-}42}$ and Pb exposure groups. Compared with the $A\beta_{1\text{-}42}$ treatment group, iNOS expression was increased significantly after the combined treatment of $A\beta_{1\text{-}42}$ and Pb (Fig. S2). To investigate the effect of microglial activation on neurons, BV-2 and HT-22 cells were co-cultured. We first examined the cell viability of HT-22 cells in the presence of Aβ and Pb. HT-22 cells were subjected to varying concentrations of $A\beta_{1\text{-}42}$ and 10 μM Pb. The results indicated that the viability of HT-22 cells decreased when exposed to higher concentrations of $A\beta_{1\text{-}42}$ (40 μM) along with 10 μM Pb (Fig. 3G). The viability of HT-22 cells was not reduced when treated with the same concentrations of $A\beta_{1\text{-}42}$ (10 μM) and Pb (10 μM) as BV-2 cells (Fig. 3G). Based on Fig. 3G, concentrations of 10 μM $A\beta_{1\text{-}42}$ and 10 μM Pb were chosen for the BV-2/HT-22 co-culture system. The results indicate that the viability of HT-22 cells in the Aβ group and the Pb group did not show a significant decrease compared to the control group. However, when $A\beta_{1\text{-}42}$ and Pb were combined, the viability of HT-22 cells was markedly lower than in both the control group and the Aβ group (Fig. 3H).

3.3. Pb exposure promotes the activation of microglia by increasing copper ion levels

Pb has been shown to increase the concentration of copper ions in cells [45], and copper can induce microglial activation through the ROS/NF-κB pathway and mitochondrial autophagy [31]. To further explore the relationship between copper homeostasis and microglial activation after Pb exposure, we detected copper ion levels in the hippocampus and in BV-2 cells. The results showed that total copper concentrations in the hippocampus were higher in the Pb-exposed groups (WT Pb group, APP/PS1 Pb group) than in the control group of the same genotype (WT control group, APP/PS1 control group) (Fig. 4A). In our in vitro experiments, the copper concentration in BV-2 cells treated with Pb and $A\beta_{1\text{-}42}$ was increased compared with that in cells treated with

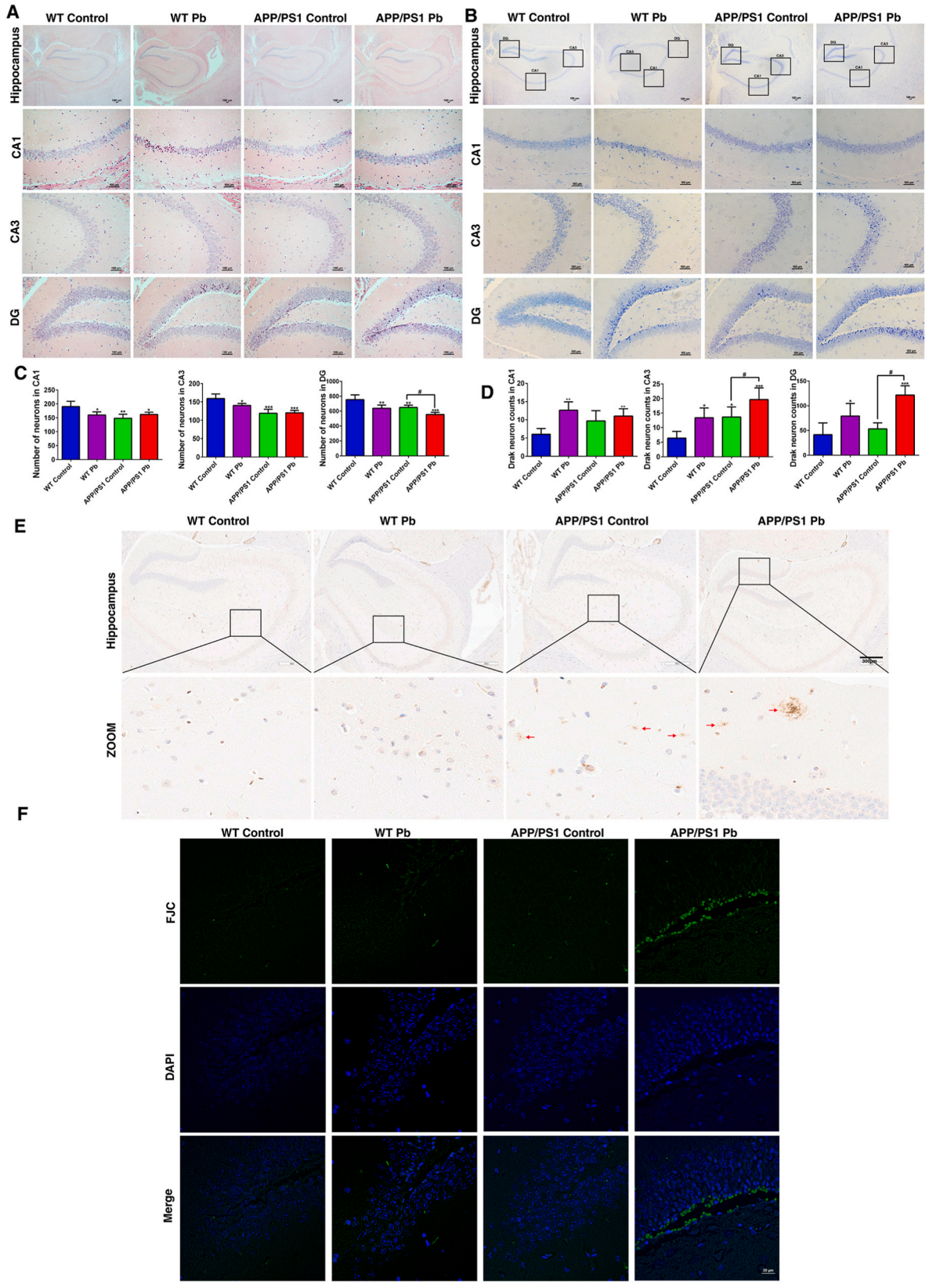

Fig. 2. Effects of Pb exposure on hippocampal neuron injury and AD pathology in APP/PS1 mice. (A) Hippocampal pathological changes of mice were observed by HE staining. (B) The damage of hippocampal neurons was detected by Nissl staining. (C–D) The number of neurons (C) and dark neurons (D) in the CA1, CA3, and DG regions. (E) Representative images of immunohistochemical labeling of Aβ to observe its deposition. Arrows point to Aβ deposition. (F) FJC staining for the detection of degenerative neurons. $^{*}P < 0.05$, $^{**}P < 0.01$, $^{***}P < 0.001$ vs. WT control group; $^{\#}P < 0.05$ vs. APP/PS1 control group.

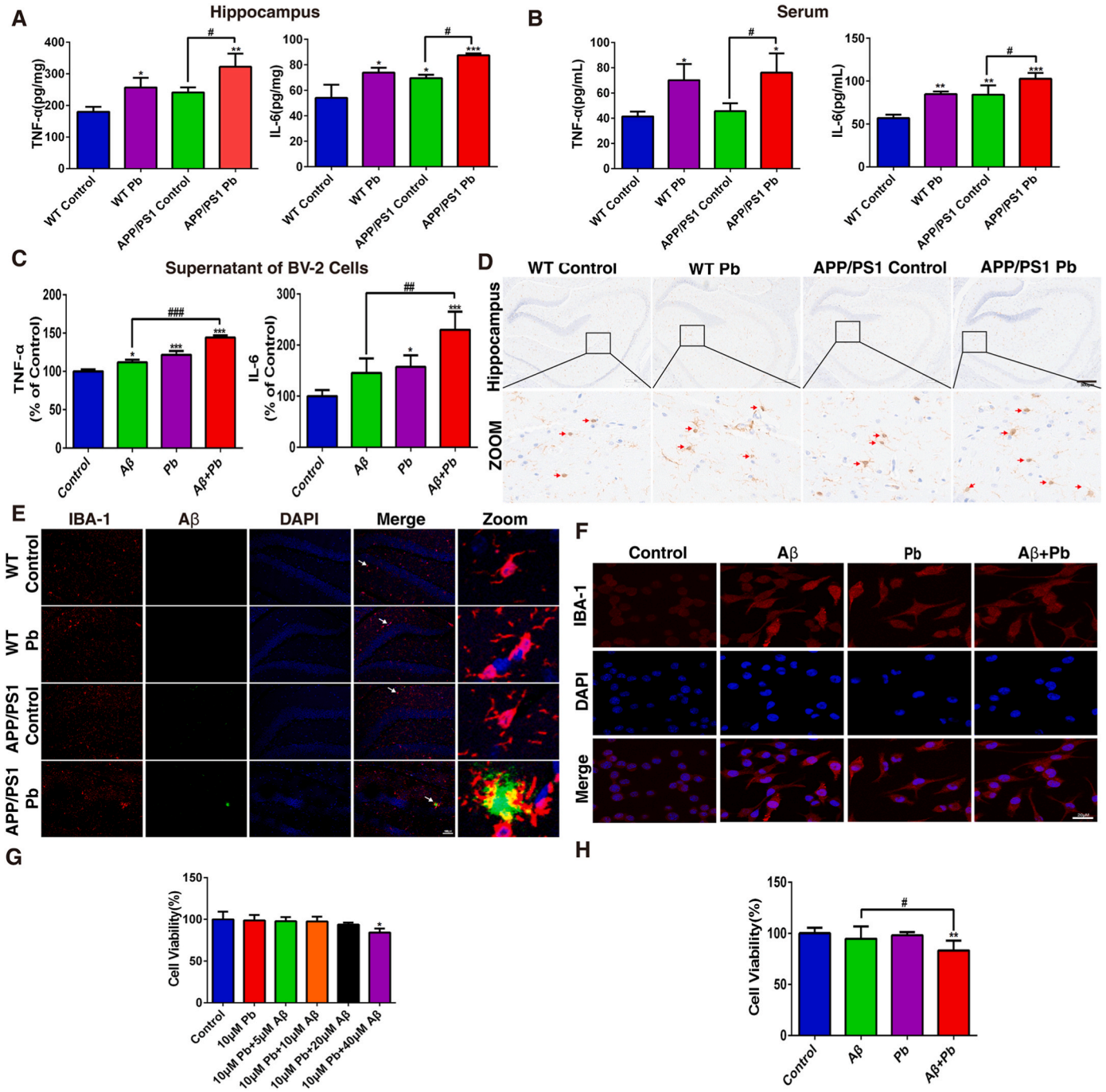

Fig. 3. Activation of microglia in AD pathology is aggravated by Pb exposure. (A) The expression levels of TNF-α and IL-6 in the hippocampus were detected by ELISA. (B) The expression levels of TNF-α and IL-6 in the serum were detected by ELISA. (C) The expression levels of TNF-α and IL-6 in the supernatant of BV-2 cells were detected by ELISA. (D) Immunohistochemical labeling of IBA-1 was used to observe the morphological changes of microglia in the hippocampus of mice. (E) The deposition of Aβ and the location of microglia in the hippocampus of mice were observed by IBA-1 and Aβ immunofluorescence double staining. (F) The morphological changes of BV-2 cells were observed by IBA-1 immunofluorescence labeling. (G) Cell survival rate of HT-22 cells treated with a concentration gradient of $A\beta_{1\text{-}42}$ (0, 5, 10, 20, and 40 μM) in combination with Pb (10 μM) using the CCK-8 assay. (H) HT-22 cell activity under co-culture conditions. $^{*}P$ <0.05, $^{**}P$ <0.01, $^{***}P$ <0.001 vs. WT control group or control group; $^{\#}P$ <0.05, $^{\#\#}P$ < 0.01, $^{\#\#\#}P$ < 0.001 vs. APP/PS1 control group or Aβ group.

$A\beta_{1\text{-}42}$ (Fig. 4B). Cells take up copper via the copper transporter CTR1 and release copper through the copper transporter ATP7A. Our Western blot results demonstrated an increase in CTR1 expression and a decrease in ATP7A expression in the hippocampus of the Pb-exposed groups (WT Pb group, APP/PS1 Pb group) compared to the same genotype control group (WT control group, APP/PS1 control group). Similarly, in BV-2 cells, the Pb group and the Aβ+Pb group exhibited an increase in CTR1 expression and a decrease in ATP7A expression compared to the control group. Compared to the Aβ group, an increase in CTR1 expression and a decrease in ATP7A expression were observed in the Aβ+Pb group (Fig. 4C and D). To investigate the relationship between microglial activation and elevated copper ion concentrations resulting from Pb exposure, we utilized a copper chelator, TM, to modulate copper levels in BV-2 cells. Our findings indicate that TM had no discernible impact on the cell viability of both BV-2 and HT-22 cells (Figs. S3A and B). The use of TM effectively reduced the levels of TNF-α and IL-6 in the supernatant

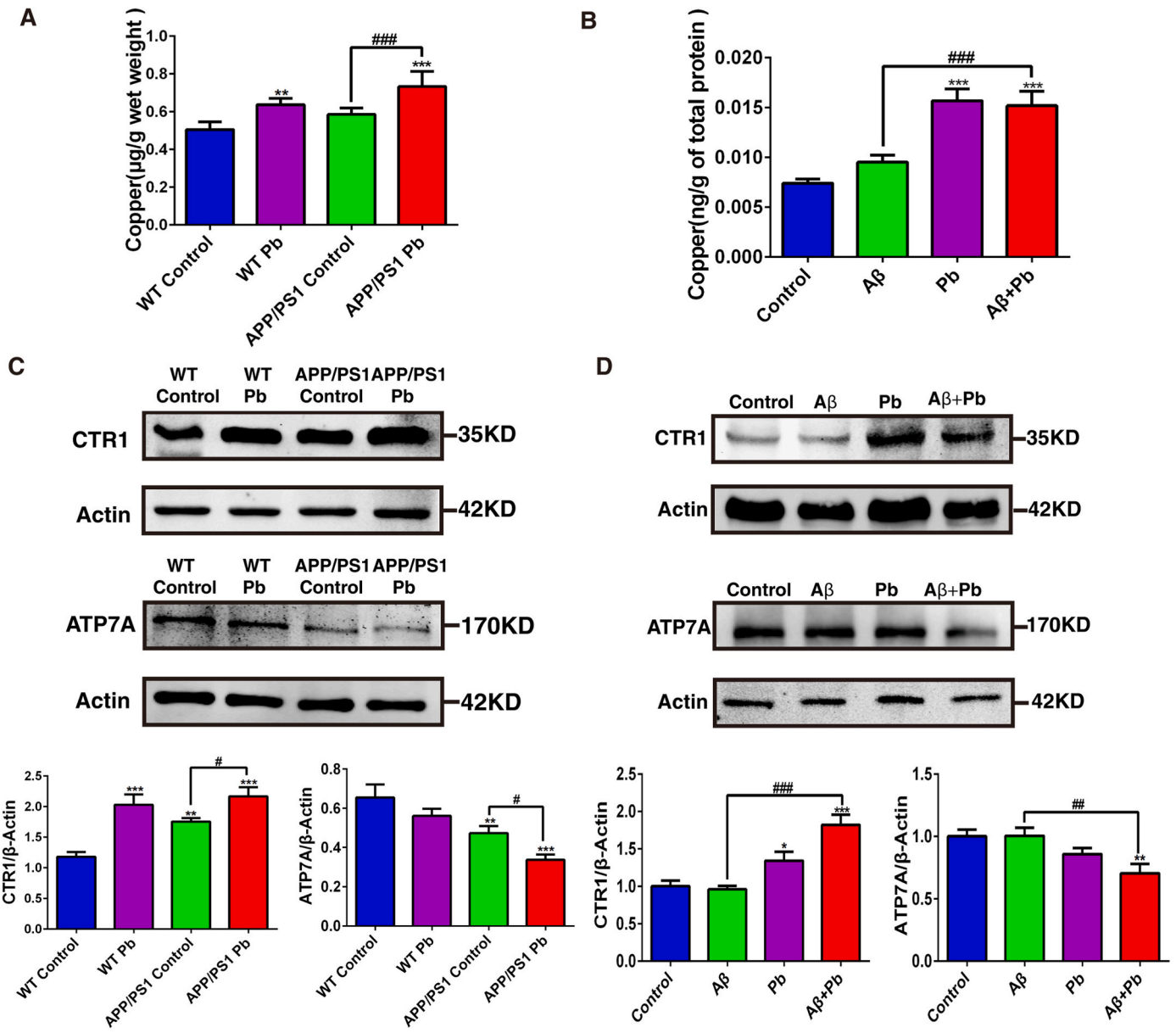

Fig. 4. Pb exposure can lead to an increase in the copper ion concentration of microglia. (A) The concentration of copper (μg/g wet weight) in the hippocampus was detected by inductively coupled plasma mass spectrometry (ICP-MS). (B) The copper concentration (ng/g of total protein) in BV-2 cells was detected by ICP-MS. (C) The expression levels of copper transporters ATP7A and CTR1 in hippocampal tissues were determined by Western blot. (D) The expression levels of copper transporters ATP7A and CTR1 in BV-2 cells were determined by Western blot.$^{*}P < 0.05$, $^{**}P < 0.01$, $^{***}P < 0.001$ vs. WT control or control group; $^{\#}P < 0.05$, $^{\#\#}P < 0.01$, $^{\#\#\#}P < 0.001$ vs. APP/PS1 control or Aβ group.

of BV-2 cells treated with Pb and Aβ (Fig. 5A). It also inhibited microglial cell body enlargement and process thickening (Fig. 5B) and reduced the expression of iNOS (Fig. S3 C), thereby effectively protecting the viability of HT-22 cells in the BV-2/HT-22 co-culture system (Fig. 5C).

3.4. Copper overload triggers mitochondrial reactive oxygen species production and mitochondrial damage, leading to microglial activation

Mitochondria are one of the main metabolic sites of copper ions in cells [40], so they are prone to damage when copper homeostasis is disrupted. Our TEM results showed that the mitochondria in the WT control group were round or oval with a normal size and distinct mitochondrial cristae, while the mitochondria in the WT Pb group showed swelling and huge vacuoles, and the mitochondrial cristae were disorganized or disappeared, suggesting mitochondrial damage. Part of the mitochondria in the APP/PS1 control group showed disordered mitochondrial cristae, while morphological changes such as mitochondrial swelling and mitochondrial ridge disappearance were more serious in the APP/PS1 Pb group (Fig. 6A). The mitochondrial membrane potential of the WT group and the APP/PS1 group decreased after Pb treatment, indicating mitochondrial damage (Fig. 6B). Compared with the $A\beta_{1\text{-}42}$ group, combined treatment with Pb affected the mitochondrial respiration of BV-2 cells. The maximum respiratory capacity and spare respiratory capacity were reduced (Fig. 6C). Compared with the $A\beta_{1\text{-}42}$ group, the mitochondrial membrane potential of BV-2 cells treated with Pb and $A\beta_{1\text{-}42}$ was significantly decreased (Fig. 6D). TM partially restored basal respiration, ATP production, proton leakage, and maximal respiration in BV-2 cells after co-treatment with Pb and $A\beta_{1\text{-}42}$, as well as the reduction of mitochondrial membrane potential induced by co-treatment with Pb and $A\beta_{1\text{-}42}$ (Fig. 6E and F). These results indicate that the mitochondrial damage caused by Pb is related to copper overload.

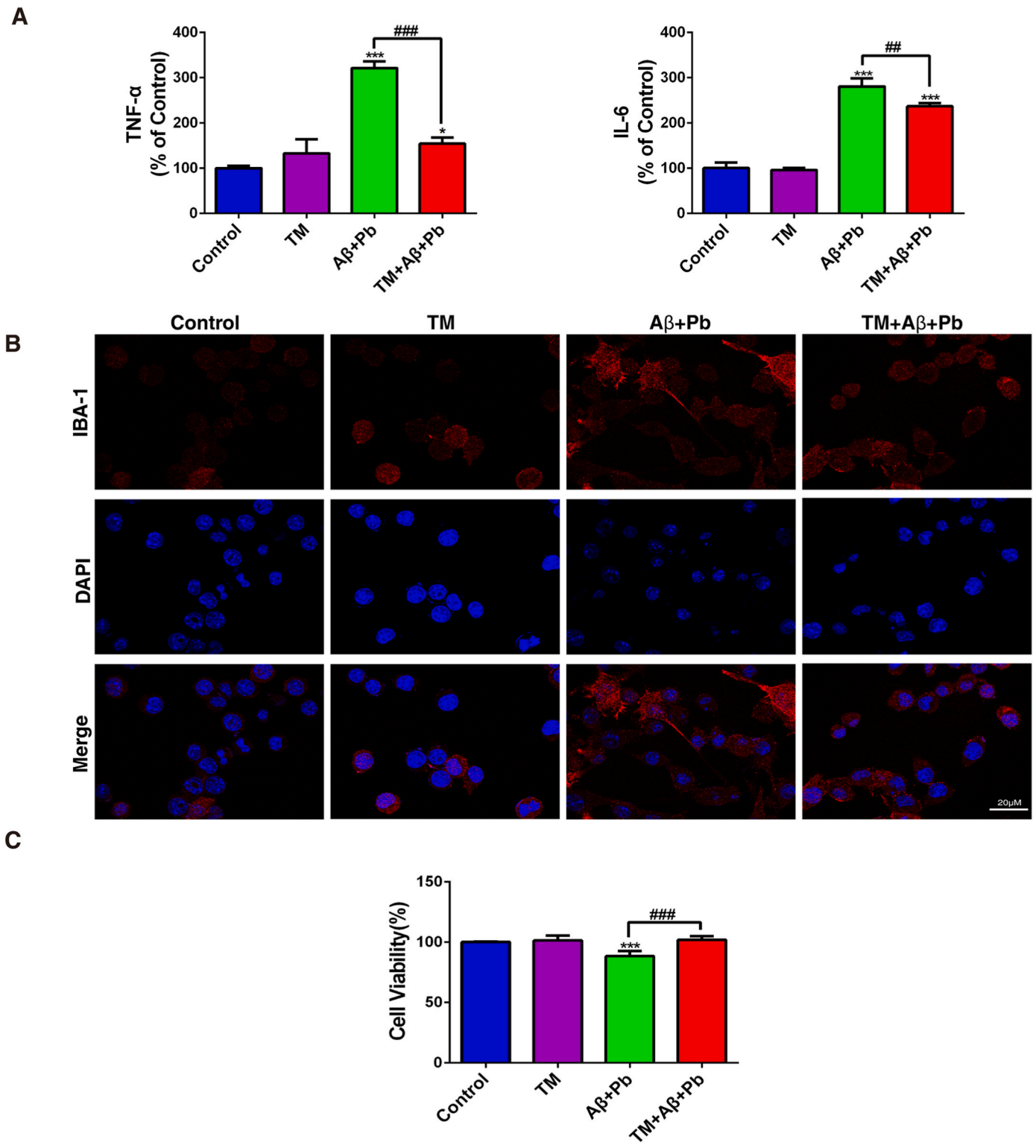

Fig. 5. Effect of changes in copper ion concentrations induced by Pb exposure on activation of microglia. (A) IBA-1 immunofluorescence staining was used to observe the morphology of BV-2 cells after TM treatment. (B) The expression of TNF-α and IL-6 in the supernatant of BV-2 cells after TM treatment was determined by ELISA. (C) CCK-8 assay to detect cell viability of HT-22 cells under co-culture conditions after TM treatment. $^{*}P < 0.05$, $^{***}P < 0.001$ vs. control group; $^{\#\#}P < 0.01$, $^{\#\#\#}P < 0.001$ vs. Aβ+Pb group.

Mitochondrial damage is closely related to mtROS, so we examined the effect of Pb on mtROS in microglia. The peroxidases (PRXs) are a family of thiol peroxidases that possess the ability to scavenge superoxide in cells. Specifically localized within mitochondria, PRX3 functions as an effective scavenger of mtROS. We observed a reduction in hippocampal PRX3 expression in the APP/PS1 Pb group compared to the APP/PS1 control group, indicating an increase in mtROS production (Fig. 7A). Combined treatment with Pb and $A\beta_{1\text{-}42}$ resulted in increased mtROS levels, and TM also effectively reduced mtROS levels (Fig. 7B and C). Administration of the mitochondrial antioxidant Mito-TEMPO was

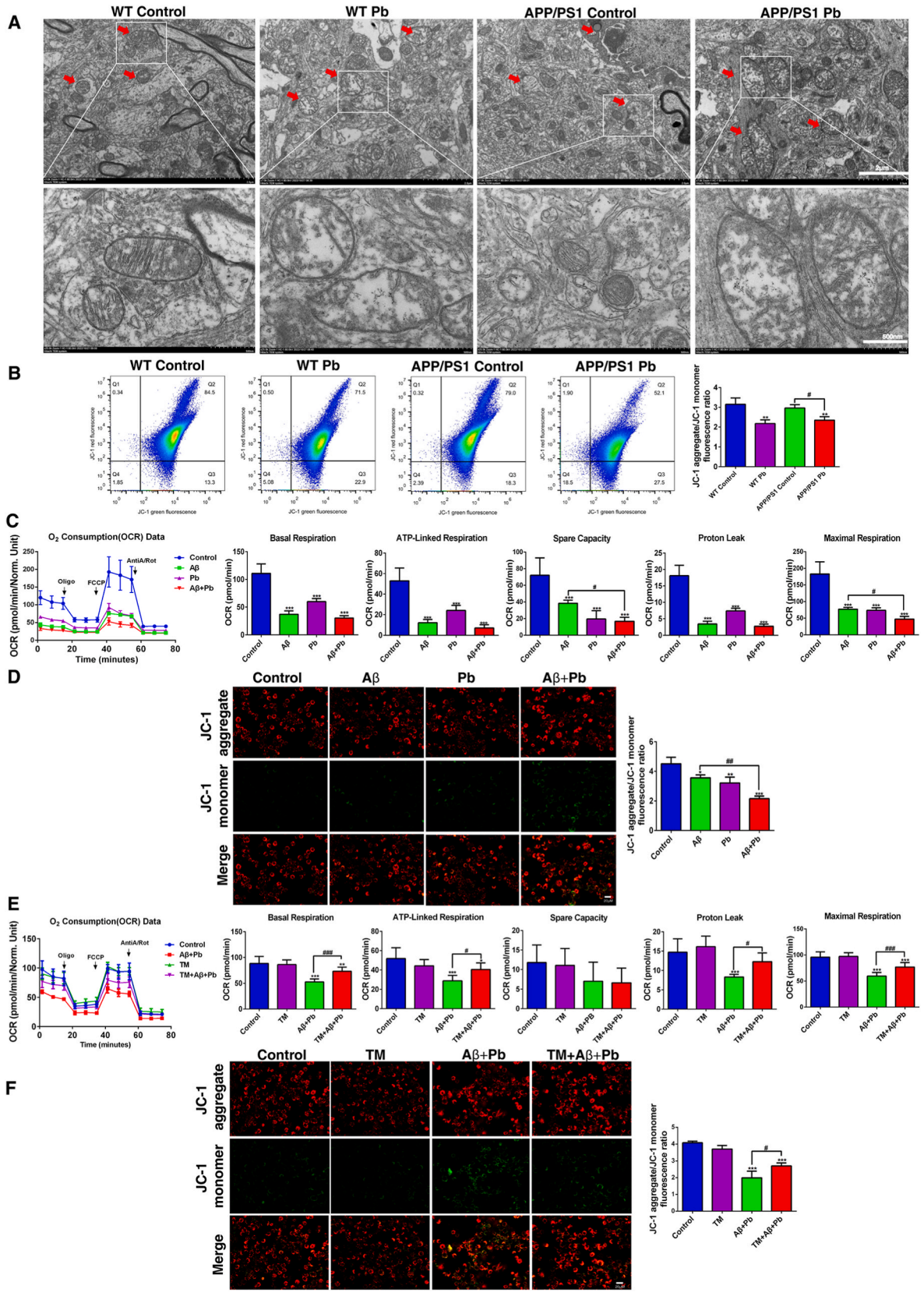

Fig. 6. Mitochondrial damage caused by copper overload. (A) Morphological changes of mitochondria in hippocampal sections of mouse brains were observed by transmission electron microscopy. (B) The mitochondrial membrane potential in the hippocampal tissue of mice was detected by JC-1 staining and assessed by flow cytometry. (C) The mitochondrial respiration of BV-2 cells was measured using Seahorse. (D) The mitochondrial membrane potential of BV-2 cells was detected by JC-1 staining. (E) Mitochondrial respiration in BV-2 cells after TM treatment was measured using Seahorse. (F) The mitochondrial membrane potential of BV-2 cells after TM treatment was detected by JC-1 staining. $^{*}P < 0.05$, $^{**}P < 0.01$, $^{***}P < 0.001$ vs. WT control or control group; $^{\#}P < 0.05$, $^{\#\#}P < 0.01$, $^{\#\#\#}P < 0.001$ vs. APP/PS1 control or Aβ group.

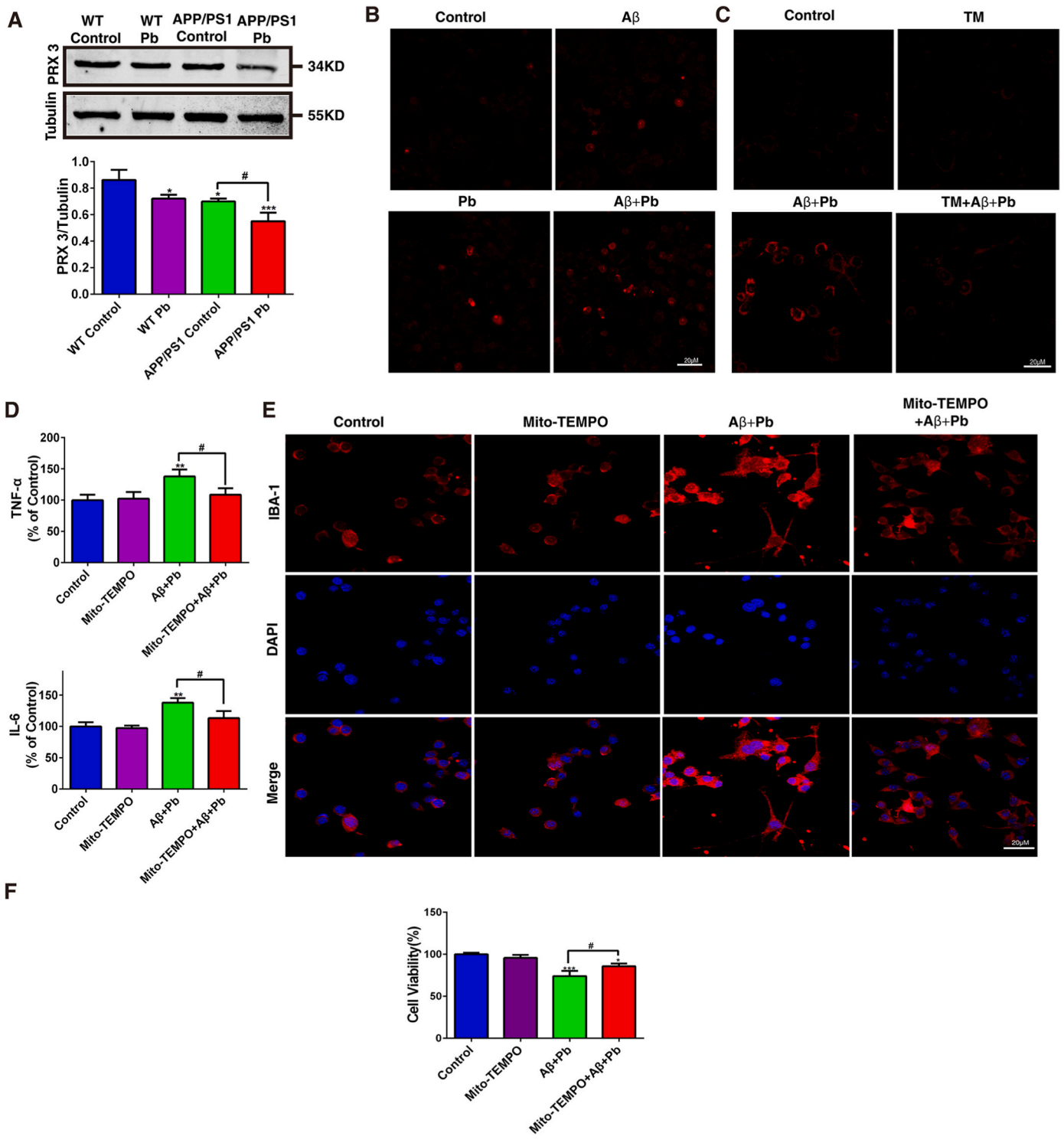

Fig. 7. Increase of mtROS due to copper overload caused by Pb exposure. (A) The expression of the anti-mitochondrial oxidation protein PRX3 was detected by Western blot. (B) mtROS levels in BV-2 cells were determined by MitoSOX. (C) mtROS levels in BV-2 cells after TM treatment were determined by MitoSOX. (D) The expression levels of TNF-α and IL-6 in the supernatant of BV-2 cells after Mito-TEMPO treatment were detected by ELISA. (E) IBA-1 immunofluorescence staining was used to observe the restoration effect of Mito-TEMPO on BV-2 cell morphology. (F) CCK-8 assay to detect cell viability of HT-22 cells under co-culture conditions after Mito-TEMPO treatment. $^{*}P < 0.05$, $^{**}P < 0.01$, $^{***}P < 0.001$ vs. WT control or control group; $^{\#}P < 0.05$, vs. APP/PS1 control or Aβ+Pb group.

found to attenuate the activation of microglia and effectively reduce the levels of TNF-α and IL-6 in the supernatants of Pb- and Aβ-treated BV-2 cells (Fig. 7D). Additionally, it inhibited microglial cell body enlargement and process thickening (Fig. 7E) and decreased iNOS expression (Fig. S4). Mito-TEMPO provides effective protection for HT-22 cells (Fig. 7F). These findings suggest that copper overload is associated with an increase in mtROS production in activated microglia.

3.5. *Mitochondrial copper induces mtROS production and then causes activation of microglia*

When the copper concentration increases, mitochondria have a

mechanism to isolate copper and transport it to mitochondrial compartments for storage [40]. Therefore, we further examined the changes in mitochondrial copper concentrations with increasing intracellular copper levels. The results showed that mitochondrial copper concentrations increased significantly upon Pb exposure (Fig. 8A and B). COX17 is responsible for transporting cytoplasmic copper to mitochondria, and the expression of COX17 in mitochondria is closely related to mitochondrial copper concentrations. The results showed that the content of COX17 in mitochondria was increased upon Pb treatment (Fig. 8C and D). Studies have shown that C-terminal truncation of COX17 can reduce the content of COX17 in mitochondria. Therefore, we established a strain stably expressing a C-terminally truncated mutant of COX17 (COX17-Δ59) and determined the mitochondrial copper concentration. COX17-Δ59 could effectively reduce the mitochondrial copper concentration of BV-2 cells but did not affect the total intracellular copper concentration, and COX17-Δ59 did not cause the activation of BV-2 cells (Fig. S5 A-G). The results demonstrate that the COX17-Δ59 + Aβ+Pb group exhibited restored basal respiration, spare capacity, and maximal respiration of mitochondria when compared to the NC-Scramble + Aβ+Pb group (Fig. 9A). Moreover, COX17-Δ59 effectively restored the decline in mitochondrial membrane potential induced by the combined treatment with Aβ and Pb (Fig. 9B) and reduced mtROS levels (Fig. 9C). These findings suggest that the damage caused by Pb exposure to mitochondria can be mitigated by reducing mitochondrial copper levels.

Reducing mitochondrial copper levels can effectively prevent mitochondrial damage and reduce the activation of microglia caused by such damage. COX17-Δ59 can also reduce the level of pro-inflammatory factors in the culture supernatant of microglia caused by the combined exposure to Aβ and Pb (Fig. 10A). Additionally, COX17-Δ59 can restore the morphological changes of microglia (Fig. 10B), reduce the expression of iNOS (Fig. S5H), and protect the neuronal cell viability in the BV-2/HT-22 co-culture system (Fig. 10D).

3.6. The increased mitochondrial import of COX17 induced by Pb exposure may be related to upregulation of the mitochondrial import protein AIF/CHCHD4

The entry of COX17 into mitochondria is aided by mitochondrial import proteins [46]. GeneMANIA predicted that there might be interactions between COX17 and CHCHD4, a mitochondrial import protein (Fig. S6). Therefore, we investigated the expression of several mitochondrial import proteins (TOMM20, TOMM40, TIMM23, PAM16, CHCHD4, and GFER) in response to Pb exposure. Our results show that the expression of CHCHD4, a mitochondrial import protein, was higher in the group treated with both Aβ and Pb compared to that in the Aβ-only group (Fig. 11A). Moreover, we observed a significant increase in the interaction between CHCHD4 and COX17 in the combined Aβ and Pb treatment group in comparison to the pure Aβ treatment group (Fig. 11B). However, the import function of CHCHD4 in mitochondria requires the involvement of AIF, a protein that also induces apoptosis. Our findings showed that the expression level of AIF followed the same trend as CHCHD4 (Fig. 11C). Furthermore, we investigated the localization of AIF and found that Pb exposure did not increase its nuclear localization (Fig. 11D). Nevertheless, the interaction between CHCHD4 and AIF was significantly higher in the combined Aβ and Pb treatment group compared to the Aβ-only group (Fig. 11E). Therefore, the increased protein expression of AIF induced by Pb exposure may be

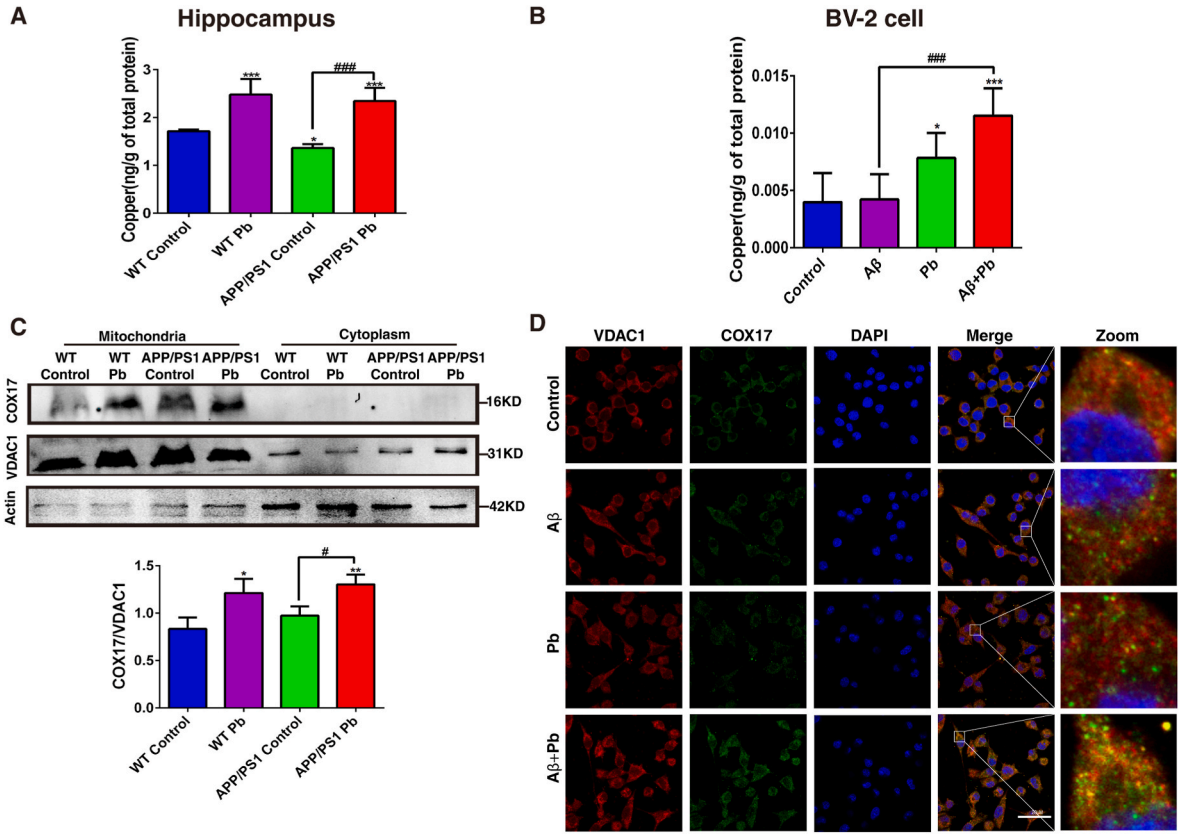

Fig. 8. Pb exposure can induce the increase of mitochondrial copper in microglia. (A) The concentration of copper (ng/g of total protein) in hippocampal mitochondria was assessed by ICP-MS. (B) The concentration of copper (ng/g of total protein) in the mitochondria of BV-2 cells was assessed by ICP-MS. (C) Expression of COX17 in hippocampal mitochondria was detected by Western blot. (D) Co-localization of COX17 (green) and VDAC1 (red), as determined using immunofluorescent labeling. $^{*}P < 0.05$, $^{**}P < 0.01$, $^{***}P < 0.001$ vs. WT control or control; $^{\#}P < 0.05$, $^{\#\#}P < 0.01$, $^{\#\#\#}P < 0.001$ vs. APP/PS1 control or Aβ group. (For interpretation of the references to colour in this figure legend, the reader is referred to the Web version of this article.)

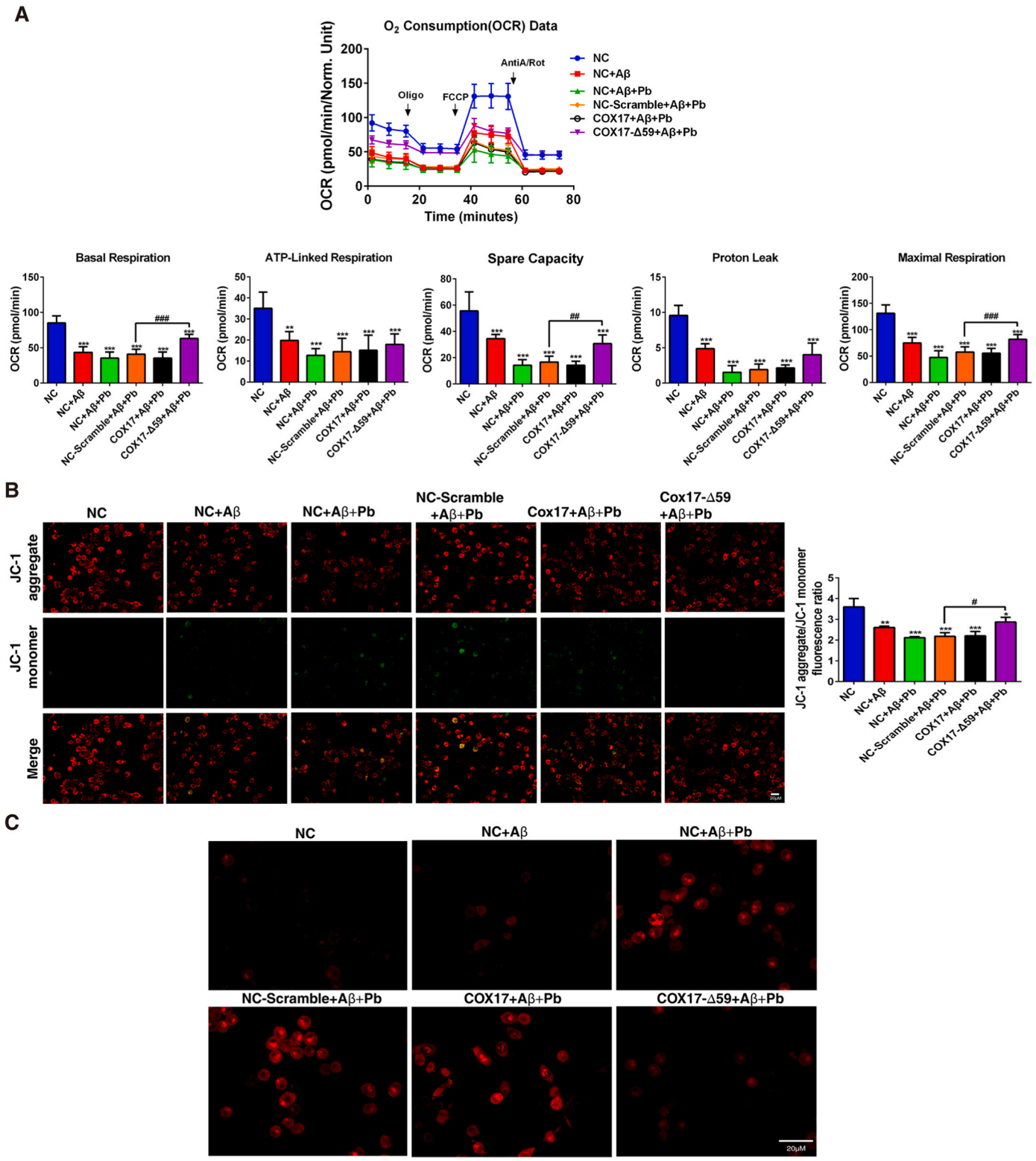

Fig. 9. Reduction of mitochondrial copper alleviated microglial activation induced by Pb. (A) The effect of the Δ59 truncated COX17 mutant on mitochondrial respiration was measured using Seahorse. (B) The effect of the Δ59 truncated COX17 mutant on the mitochondrial membrane potential was detected using JC-1 staining. (C) The effect of the Δ59 truncated COX17 mutant on mtROS levels was detected by MitoSOX. NC: negative control group without lentivirus infection. NC-Scramble: negative control group with vector lentivirus infection. $^{*}P < 0.05$, $^{**}P < 0.01$, $^{***}P < 0.001$ vs. WT control, control, or NC group; $^{\#}P < 0.05$, $^{\#\#}P < 0.01$, $^{\#\#\#}P < 0.001$ vs. APP/PS1 control, Aβ, or NC-Scramble + Aβ+Pb group.

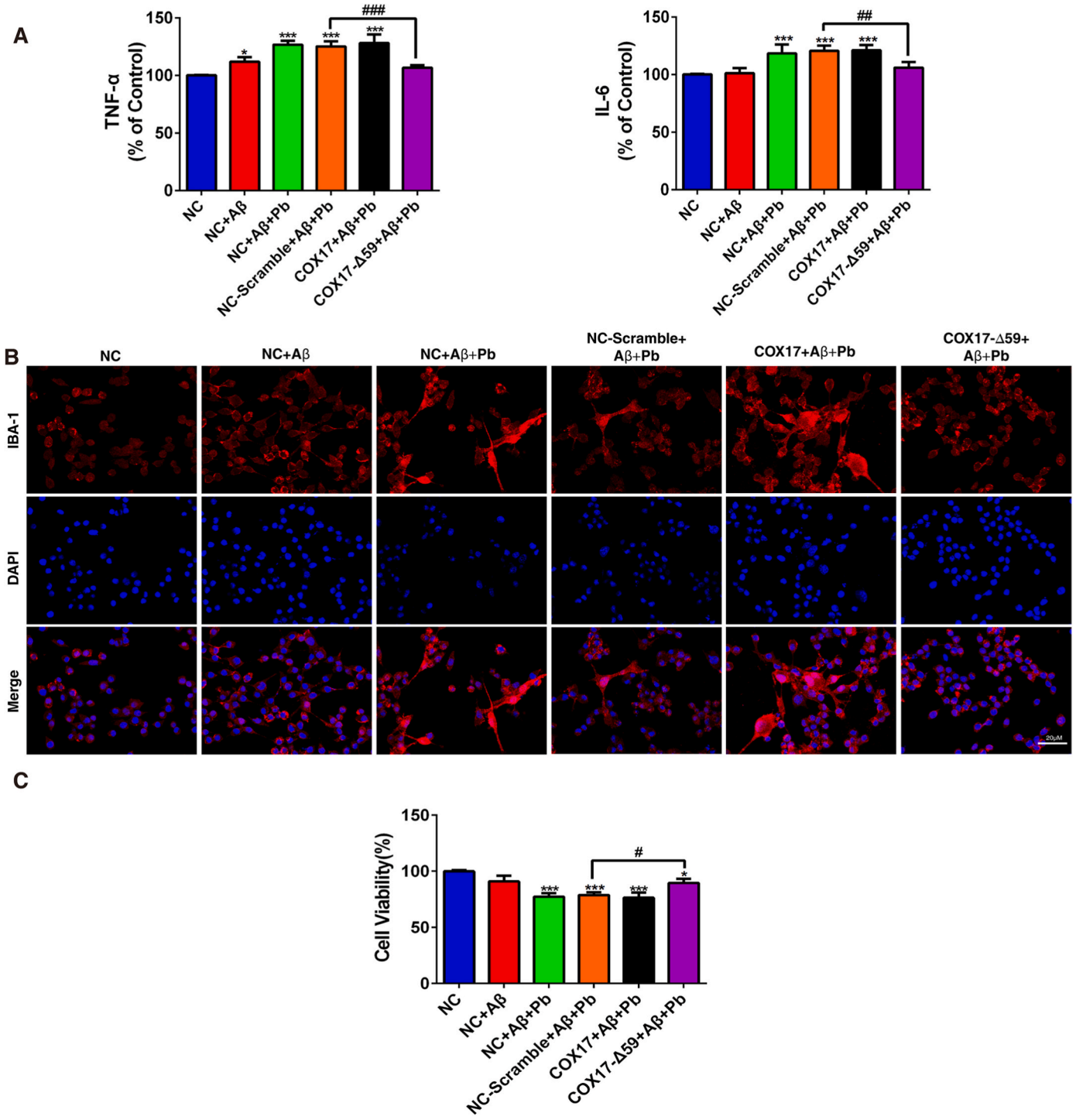

Fig. 10. Pb exposure increased mitochondrial copper, resulting in the activation of microglia. (A) The expression levels of TNF-α and IL-6 in the supernatant of cells expressing the Δ59 truncated COX17 mutant were detected by ELISA. (B) IBA-1 immunofluorescence staining was used to observe the morphological recovery effect of the Δ59 truncated COX17 mutant on BV-2 cells. (C) The activity of HT-22 cells under co-culture conditions after expression of the Δ59 truncated COX17 mutant was detected by CCK-8 assay. NC: negative control group without lentivirus infection. NC-Scramble: negative control group with vector lentivirus infection. $^{*}P < 0.05$, $^{***}P < 0.001$ vs. NC group; $^{\#}P < 0.05$, $^{\#\#}P < 0.01$, $^{\#\#\#}P < 0.001$ vs. NC-Scramble + Aβ+Pb group.

involved in mitochondrial import of COX17 together with CHCHD4.

4. Discussion

In this study, we report that mitochondrial copper overload in microglia mediates Pb-induced learning and memory impairment in APP/PS1 mice. Our findings indicate that Pb exposure can enhance the movement of COX17 to the mitochondria by increasing the expression of the mitochondrial import protein AIF/CHCHD4. This leads to excessive copper accumulation in the mitochondria. The build-up of copper in the mitochondria can cause damage to these organelles and the generation of mtROS. Consequently, the activation of microglia is triggered, further exacerbating neuronal damage.

Pb is considered an environmental risk factor that is closely linked to

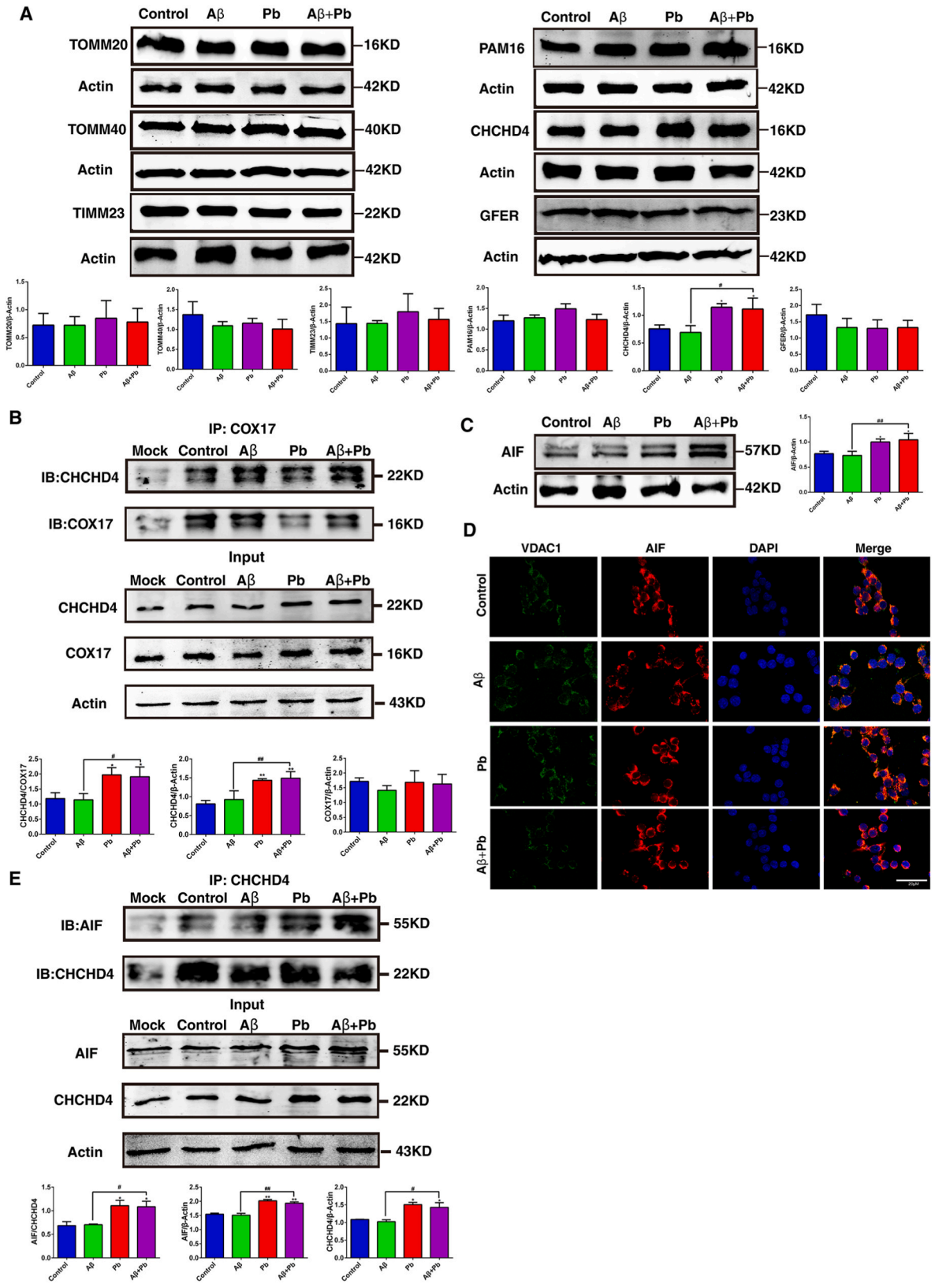

Fig. 11. Pb exposure upregulated the MIA mitochondrial import pathway, which may be related to increased mitochondrial import of COX17. (A) The expression levels of mitochondrial import proteins (TOMM20, TOMM40, TIMM23, PAM16, CHCHD4, and GFER) were determined by Western blot. (B) The interaction of COX17 and CHCHD4 was detected by co-immunoprecipitation. (C) The expression of AIF was detected by Western blot. (D) Localization of AIF was observed by immunofluorescence. (E) The interaction of AIF and CHCHD4 was detected by co-immunoprecipitation. $*P < 0.05$, $**P < 0.01$ vs. control group; $\#P < 0.05$, $\#\#P < 0.01$ vs. Aβ group.

AD. Studies have revealed that the blood Pb level of individuals with AD is significantly higher than that of controls [47]. In a study that examined the impact of Pb on AD neuropathology, it was discovered that exposure to low concentrations of Pb in early life resulted in increased levels of APP and Aβ in the brains of rats in later life [48]. To further investigate the relationship between Pb and AD, we used the APP/PS1 mouse model, which is widely used as a model for AD studies because they develop classic symptoms of AD early in life, such as learning and memory impairments and Aβ deposition. These transgenic mice develop AD-like pathology with Aβ deposition, impaired short-term memory, and impaired long-term potentiation at 3 months of age [49]. A previous study has confirmed that Pb exposure can cause abnormal changes in the blood–brain barrier and activate astrocytes, thus aggravating AD pathology [22]. According to the China Environmental Survey [50], the Pb concentration in the Pearl River system exceeds 90 ppm. Based on this finding, the exposure concentration of mice was set to 100 ppm. APP/PS1 mice were subjected to chronic Pb exposure from the post-weaning developmental period (3 weeks of age) until the age of 4 months to observe whether Pb exposure accelerated the progression of AD pathology. The results showed that continuous exposure to 100 ppm Pb increased blood and brain Pb concentrations in the model, so the Pb exposure mouse model was established successfully. Meanwhile, after Pb exposure, the results of the MWM test and the NOR test showed that APP/PS1 mice had an impaired learning and memory ability, increased Aβ plaque deposits, and more severe neuronal damage in the hippocampus. These results suggest that Pb exposure can aggravate AD in APP/PS1 mice.

Microglia are specialized macrophages of the CNS. When microglia are in a stable state, they maintain communication with astrocytes and neuronal cells. In the presence of external stimuli, microglia can be rapidly activated to maintain homeostasis in the CNS [51]. When microglia are activated, expression of iNOS producing NO and derivative oxidants, Both increased inflammatory factors and morphological changes can be considered as markers of microglial activation [52]. Pb has been shown to activate BV-2 cells and increase the secretion of IL-1β, TNF-α, and IL-6 [53]. A study has shown that AD patients often have neuroinflammatory symptoms [54]. It has been proved that the increase in Aβ deposition is closely related to the activation of microglia in AD models [55]. Our in vitro experiments confirmed that Pb can increase the activation of BV-2 cells under Aβ treatment, promote the expression of iNOS and the secretion of the inflammatory cytokines TNF-α and IL-6, and decrease neuronal cell activity in a co-culture system, suggesting that Pb can exacerbate neuronal damage in the AD model by inducing microglial activation and subsequent release of inflammatory factors, thereby worsening AD pathology.

Copper is an essential element for enzymes such as ULK1, Cu/Zn-SOD1, and MEK1, which play significant roles in neurite elongation and maintenance of redox balance [56,57]. The high-affinity copper uptake protein CTR1 is responsible for cellular copper uptake, and ATP7A regulates cellular copper efflux by catalyzing the transfer of copper on the cell membrane [58,59]. Changes in CTR1 and ATP7A expression may disrupt intracellular copper homeostasis, leading to disease. Such disruptions have also been observed in AD [60,61]. In our study, we found that Pb can upregulate CTR1 and downregulate ATP7A in hippocampal tissues and BV-2 cells. In addition, Pb exposure can cause an increase in copper concentrations. A study found that exposure to copper resulted in the activation of microglia in mice [31]. However, we discovered that the use of copper chelators can alleviate microglial activation, indicating that Pb promotes microglial activation by increasing the copper concentration. A previous study has shown that Pb can increase the copper content in the brains of mice [27]; however, research on the damage to the nervous system caused by this increase is limited. Our study found that Pb can promote the activation of microglia by increasing the copper concentration, which further worsens the learning and memory impairment of APP/PS1 mice. Additionally, excess copper in the cytoplasm may promote the production and deposition of Aβ peptide through its participation in the cleavage of APP. Previous studies have demonstrated that hCTR1 mRNA plays a role in cellular copper metabolism by regulating the expression of CTR1. The transcription factor SP1 is responsible for the regulation of hCTR1 mRNA [62]. In addition, SP1 is involved in the regulation of APP in Pb-induced neurodegeneration [63], and is closely associated with neurodegenerative diseases linked to epigenetic regulation [64]. Pb, as an environmental risk factor show a association of tibial lead concentration with cognitive decline in adults [65], has been shown to impact epigenetic regulation [5,66]. Our data also indicate that Pb can impact intracellular copper balance through epigenetic modification (data not shown). Further research is needed to investigate whether Pb affects SP1 through epigenetic mechanisms, leading to changes in hCTR1 mRNA and other AD-related genes. These changes may contribute to cellular copper ion imbalance and the development of AD-related pathological changes.

A previous study has shown that mitochondrial copper can promote the expression of inflammatory genes in macrophages [67]. Our current study found that Pb exposure increased mitochondrial copper levels in the hippocampus of APP/PS1 mice and in the BV-2 cell line, along with increased mitochondrial localization of the mitochondrial copper transporter COX17. The activation of microglia can be reduced by lowering the concentration of mitochondrial copper. In cases where copper homeostasis is disrupted, the mitochondria can play a role by reducing cytoplasmic copper levels [40]. This helps to reduce the associated toxicity, but it also increases the likelihood of mitochondrial damage [40]. Therefore, mitochondria are prone to damage when copper homeostasis is disrupted. COX17 exists in the intermembrane space between the cytoplasm and mitochondria and is responsible for transporting copper ions from the cytoplasm to the respiratory chain complex [39]. The expression of COX17 in mitochondria is closely related to the mitochondrial copper concentration [68]. Our results showed that after exposure to Pb in cells, mitochondrial translocation of COX17 increased, followed by an increase in mitochondrial copper concentration, and this mitochondrial copper overload caused mitochondrial morphological damage, affected oxidative phosphorylation, reduced the mitochondrial membrane potential, and exacerbated mitochondrial oxidative stress. This damage was mitigated by copper-chelating agents or by reducing the mitochondrial translocation of COX17. A previous study has reported that more than 99 % of mitochondrial proteins are imported into the mitochondria through different mitochondrial import pathways, such as the presequence pathway, the carrier pathway, the β-barrel pathway, the mitochondrial intermembrane space import and assembly (MIA) pathway, and outer membrane proteins with α-helical transmembrane segments in the mitochondrial membrane and intermembrane space [69]. The MIA pathway consists of the FDA-dependent mercaptooxidase GFER and Mia40/CHCHD4 import receptors [46]. A study indicated that COX17 translocation to mitochondria increases significantly when the MIA pathway is activated [70], which is consistent with our results, showing that AIF/CHCHD4 expression and COX17 translocation to mitochondria were increased after Pb treatment. The accumulation of mitochondrial copper, caused by an increase in COX17 levels in mitochondria, can lead to mitochondrial damage. This damage is closely related to an increase in mtROS. Furthermore, mitochondrial damage can cause an increase in mtROS, which in turn exacerbates the damage to the mitochondria [71]. Additionally, an increase in mtROS can induce the activation of microglia [72]. Our study found that the production of mtROS was involved in the activation process of microglia in APP/PS1 mice and in vitro models after exposure to Pb. Previous studies have demonstrated that Pb exposure contributes to the development of AD by leading to neuronal damage and activating astrocytes [22]. Our findings suggest that Pb exposure can promote the translocation of COX17 to the mitochondria by upregulating the expression of the mitochondrial import protein AIF/CHCHD4. As a result, excessive accumulation of copper occurs in the mitochondria, which can lead to organelle damage and the production of mtROS. This series of events ultimately triggers microglia

activation, which further aggravates neuronal damage and ultimately leads to the worsening of AD pathology. However, the mechanism by which Pb promotes increased expression of mitochondrial import proteins still requires further investigation. Previous studies have demonstrated that early Pb exposure may result in the overexpression of AD-related genes later in life [73], and the epigenome-based latent early-life associated regulation (LEARn) focused on the effects that accumulated environmental hits may provide a mechanistic explanation for sporadic AD caused by this gene-environment interaction [74,75].

In this study, we demonstrated that chronic Pb exposure can aggravate learning and memory impairment in APP/PS1 mice. The mechanism may be related to increased expression of the mitochondrial protein CHCHD4/AIF in microglia, which leads to mitochondrial copper overload in mitochondria due to COX17-mediated translocation, thus inducing mitochondrial dysfunction and excessive mtROS accumulation, promoting the activation of microglia. This study is the first to reveal the role of microglial activation caused by mitochondrial copper overload in microglia in Pb-aggravated AD-like pathology.

Author contribution statement

Dingbang Huang: Methodology, performed experiments, Writing-original draft, Writing-review & editing.

Lixuan Chen: Performed experiments, Writing-original draft, Writing-review & editing.

Qiuyi Ji, Yang Xiang, Qin Zhou, Kaiju Chen, Xiaoshun Zhang: Investigation, Performed experiments.

Fei Zou: Conceptualization, Supervision.

Xingmei Zhang, Zaihua Zhao, Tao Wang: Conceptualization, Writing-review & editing.

Gang Zheng: Conceptualization, Supervision, Writing-review & editing.

Xiaojing Meng: Conceptualization, Methodology, Supervision, Writing-review & editing.

Declaration of competing interest

The authors declare that they have no conflict of interest.

Data availability

No data was used for the research described in the article.

Acknowledgments

This work was supported by the National Natural Science Foundation of China (Grant Nos. 81920108030, 81973071, 82130054), Guangdong Basic and Applied Basic Research Foundation (No. 2023A1515012500, 2023A1515011148). The funding bodies were not involved in the study design; collection, analysis, interpretation of data; and writing the manuscript. We thank LetPub (www.letpub.com) for its linguistic assistance during the preparation of this manuscript.

Appendix A. Supplementary data

Supplementary data to this article can be found online at https://doi.org/10.1016/j.redox.2023.102990.

References

[1] H. Gu, P.R. Territo, S.A. Persohn, A.A. Bedwell, K. Eldridge, R. Speedy, et al., Evaluation of chronic lead effects in the blood brain barrier system by DCE-CT, J. Trace Elem. Med. Biol. 62 (2020), 126648.

[2] Y. Bai, A. Laenen, V. Haufroid, T.S. Nawrot, B. Nemery, Urinary lead in relation to combustion-derived air pollution in urban environments. A longitudinal study of an international panel, Environ. Int. 125 (2019) 75–81.

[3] P. Jarvis, K. Quy, J. Macadam, M. Edwards, M. Smith, Intake of lead (Pb) from tap water of homes with leaded and low lead plumbing systems, Sci. Total Environ. 644 (2018) 1346–1356.

[4] M.A. Laidlaw, G.M. Filippelli, R.C. Sadler, C.R. Gonzales, A.S. Ball, H.W. Mielke, Children's blood lead seasonality in flint, Michigan (USA), and soil-sourced lead hazard risks, Int. J. Environ. Res. Publ. Health 13 (2016) 358.

[5] D. Cuomo, M.J. Foster, D. Threadgill, Systemic review of genetic and epigenetic factors underlying differential toxicity to environmental lead (Pb) exposure 29 (2022) 35583–35598.

[6] J.H. Kim, C.W. Oh, J.C. Kang, Antioxidant responses, neurotoxicity, and metallothionein gene expression in juvenile Korean rockfish Sebastes schlegelii under dietary lead exposure, J. Aquat. Anim. Health 29 (2017) 112–119.

[7] Y. Chen, G. Mao, Z. Zhang, T. Zhao, W. Feng, L. Yang, et al., The protective effect of C3G against Pb-induced learning and memory impairments through cAMP-PKA-CREB signaling pathway in rat hippocampus, Process Biochem. 118 (2022) 381–393.

[8] J. Zhu, F. Zhou, Q. Zhou, Y. Xu, Y. Li, D. Huang, et al., NLRP3 activation in microglia contributes to learning and memory impairment induced by chronic lead exposure in mice, Toxicol. Sci. 191 (2023) 179–191.

[9] S.W. Bihaqi, A. Bahmani, G.M. Subaiea, N.H. Zawia, Infantile exposure to lead and late-age cognitive decline: relevance to AD, Alzheimers Dement 10 (2014) 187–195.

[10] M.G. Weisskopf, J. Weuve, H. Nie, M.H. Saint-Hilaire, L. Sudarsky, D.K. Simon, et al., Association of cumulative lead exposure with Parkinson's disease, Environ. Health Perspect. 118 (2010) 1609–1613.

[11] D.S. Knopman, H. Amieva, R.C. Petersen, G. Chételat, D.M. Holtzman, B.T. Hyman, et al., Alzheimer disease, Nat. Rev. Dis. Prim. 7 (2021) 33.

[12] W. Jagust, Imaging the evolution and pathophysiology of Alzheimer disease, Nat. Rev. Neurosci. 19 (2018) 687–700.

[13] M.A. DeTure, D.W. Dickson, The neuropathological diagnosis of Alzheimer's disease, Mol. Neurodegener. 14 (2019) 32.

[14] S. Tiwari, V. Atluri, A. Kaushik, A. Yndart, M. Nair, Alzheimer's disease: pathogenesis, diagnostics, and therapeutics, Int. J. Nanomed. 14 (2019) 5541–5554.

[15] T. Guo, D. Zhang, Y. Zeng, T.Y. Huang, H. Xu, Y. Zhao, Molecular and cellular mechanisms underlying the pathogenesis of Alzheimer's disease, Mol. Neurodegener. 15 (2020) 40.

[16] M. Fakhoury, Microglia and astrocytes in Alzheimer's disease: implications for therapy, Curr. Neuropharmacol. 16 (2018) 508–518.

[17] A. Katsumoto, H. Takeuchi, K. Takahashi, F. Tanaka, Microglia in Alzheimer's disease: risk factors and inflammation, Front. Neurol. 9 (2018) 978.

[18] M. Prinz, S. Jung, J. Priller, Microglia biology: one century of evolving concepts, Cell 179 (2019) 292–311.

[19] K.M. Bakulski, J.F. Dou, R.C. Thompson, C. Lee, L.Y. Middleton, B.P.U. Perera, et al., Single-cell analysis of the gene expression effects of developmental lead (Pb) exposure on the mouse Hippocampus, Toxicol. Sci. 176 (2020) 396–409.

[20] P. Su, D. Wang, Z. Cao, J. Chen, J. Zhang, The role of NLRP3 in lead-induced neuroinflammation and possible underlying mechanism, Environ. Pollut. 287 (2021), 117520.

[21] X. Liu, Y. Chen, H. Wang, Y. Wei, Y. Yuan, Q. Zhou, et al., Microglia-derived IL-1β promoted neuronal apoptosis through ER stress-mediated signaling pathway PERK/eIF2α/ATF4/CHOP upon arsenic exposure, J. Hazard Mater. 417 (2021), 125997.

[22] S. Wu, H. Liu, H. Zhao, X. Wang, J. Chen, D. Xia, et al., Environmental lead exposure aggravates the progression of Alzheimer's disease in mice by targeting on blood brain barrier, Toxicol. Lett. 319 (2020) 138–147.

[23] L. Frölich, A. Atri, C. Ballard, P.N. Tariot, J.L. Molinuevo, N. Boneva, et al., Open-label, multicenter, phase III extension study of idalopirdine as adjunctive to donepezil for the treatment of mild-moderate Alzheimer's disease, J Alzheimers Dis 67 (2019) 303–313.

[24] Kumar R. Himani, J.A. Ansari, A.A. Mahdi, D. Sharma, B. Karunanand, et al., Blood lead levels in occupationally exposed workers involved in battery factories of Delhi-NCR region: effect on vitamin D and calcium metabolism, Indian J. Clin. Biochem. 35 (2020) 80–87.

[25] A. Garza, R. Vega, E. Soto, Cellular mechanisms of lead neurotoxicity, Med Sci Monit 12 (2006) Ra57–65.

[26] S. Li, C. Yang, X. Yi, R. Wei, M. Aschner, Y. Jiang, et al., Effects of sub-chronic lead exposure on essential element levels in mice, Biol. Trace Elem. Res. 201 (2023) 282–293.

[27] B. He, L. Wang, S. Li, F. Cao, L. Wu, S. Chen, et al., Brain copper clearance by the blood-cerebrospinal fluid-barrier: effects of lead exposure, Neurosci. Lett. 768 (2022), 136365.

[28] A. Rahman, K.M. Khan, M.S. Rao, Exposure to low level of lead during preweaning period increases metallothionein-3 expression and dysregulates divalent cation levels in the brain of young rats, Neurotoxicology 65 (2018) 135–143.

[29] G. Zheng, J. Zhang, Y. Xu, X. Shen, H. Song, J. Jing, et al., Involvement of CTR1 and ATP7A in lead (Pb)-induced copper (Cu) accumulation in choroidal epithelial cells, Toxicol. Lett. 225 (2014) 110–118.

[30] S. Lutsenko, C. Washington-Hughes, M. Ralle, K. Schmidt, Copper and the brain noradrenergic system, J. Biol. Inorg. Chem. 24 (2019) 1179–1188.

[31] Q. Zhou, Y. Zhang, L. Lu, H. Zhang, C. Zhao, Y. Pu, et al., Copper induces microglia-mediated neuroinflammation through ROS/NF-κB pathway and mitophagy disorder, Food Chem. Toxicol. 168 (2022), 113369.

[32] L. Wang, Y.L. Yin, X.Z. Liu, P. Shen, Y.G. Zheng, X.R. Lan, et al., Current understanding of metal ions in the pathogenesis of Alzheimer's disease, Transl. Neurodegener. 9 (2020) 10.

[33] M.T. Kabir, M.S. Uddin, S. Zaman, Y. Begum, G.M. Ashraf, M.N. Bin-Jumah, et al., Molecular mechanisms of metal toxicity in the pathogenesis of Alzheimer's disease, Mol. Neurobiol. 58 (2021) 1–20.
[34] R. Squitti, I. Simonelli, M. Ventriglia, M. Siotto, P. Pasqualetti, A. Rembach, et al., Meta-analysis of serum non-ceruloplasmin copper in Alzheimer's disease, J Alzheimers Dis 38 (2014) 809–822.
[35] S. Bucossi, M. Ventriglia, V. Panetta, C. Salustri, P. Pasqualetti, S. Mariani, et al., Copper in Alzheimer's disease: a meta-analysis of serum,plasma, and cerebrospinal fluid studies, J Alzheimers Dis 24 (2011) 175–185.
[36] R. Squitti, Copper subtype of Alzheimer's disease (AD): meta-analyses, genetic studies and predictive value of non-ceruloplasmim copper in mild cognitive impairment conversion to full AD, J. Trace Elem. Med. Biol. 28 (2014) 482–485.
[37] R. Squitti, M. Ventriglia, I. Simonelli, Copper Imbalance in Alzheimer's Disease: Meta-Analysis of Serum, Plasma, and Brain Specimens, and Replication Study Evaluating ATP7B Gene Variants, vol. 11, 2021.
[38] K. Li, A. Li, Y. Mei, J. Zhao, Q. Zhou, Y. Li, et al., Trace elements and Alzheimer dementia in population-based studies: a bibliometric and meta-analysis, Environ. Pollut. 318 (2023), 120782.
[39] J. Chen, Y. Jiang, H. Shi, Y. Peng, X. Fan, C. Li, The molecular mechanisms of copper metabolism and its roles in human diseases, Pflueg. Arch. Eur. J. Physiol. 472 (2020) 1415–1429.
[40] P.A. Cobine, S.A. Moore, S.C. Leary, Getting out what you put in: copper in mitochondria and its impacts on human disease, Biochim. Biophys. Acta Mol. Cell Res. 1868 (2021), 118867.
[41] M.L. Calió, A.C. Mosini, D.S. Marinho, G.N. Salles, F.H. Massinhani, G.M. Ko, et al., Leptin enhances adult neurogenesis and reduces pathological features in a transgenic mouse model of Alzheimer's disease, Neurobiol. Dis. 148 (2021), 105219.
[42] A.B. Maxfield, D.N. Heaton, D.R. Winge, Cox17 is functional when tethered to the mitochondrial inner membrane, J. Biol. Chem. 279 (2004) 5072–5080.
[43] H. Ooigawa, H. Nawashiro, S. Fukui, N. Otani, A. Osumi, T. Toyooka, et al., The fate of Nissl-stained dark neurons following traumatic brain injury in rats: difference between neocortex and hippocampus regarding survival rate, Acta Neuropathol. 112 (2006) 471–481.
[44] I. Plastira, E. Bernhart, M. Goeritzer, H. Reicher, V.B. Kumble, N. Kogelnik, et al., 1-Oleyl-lysophosphatidic acid (LPA) promotes polarization of BV-2 and primary murine microglia towards an M1-like phenotype, J. Neuroinflammation 13 (2016) 205.
[45] Y. Liu, Z.H. Zhao, T. Wang, J.Y. Yao, W.Q. Wei, L.H. Su, et al., Lead exposure disturbs ATP7B-mediated copper export from brain barrier cells by inhibiting XIAP-regulated COMMD1 protein degradation, Ecotoxicol. Environ. Saf. 256 (2023), 114861.
[46] S. Goyal, S. Tiwari, B. Seth, A. Tandon, J. Shankar, M. Sinha, et al., Bisphenol-A inhibits mitochondrial biogenesis via impairment of GFER mediated mitochondrial protein import in the rat brain hippocampus, Neurotoxicology 85 (2021) 18–32.
[47] B. Fathabadi, M. Dehghanifiroozabadi, J. Aaseth, G. Sharifzadeh, S. Nakhaee, A. Rajabpour-Sanati, et al., Comparison of blood lead levels in patients with Alzheimer's disease and healthy people 33 (2018) 541–547.
[48] M.R. Basha, W. Wei, S.A. Bakheet, N. Benitez, H.K. Siddiqi, Y.W. Ge, et al., The fetal basis of amyloidogenesis: exposure to lead and latent overexpression of amyloid precursor protein and beta-amyloid in the aging brain, J. Neurosci. 25 (2005) 823–829.
[49] D. Puzzo, W. Gulisano, A. Palmeri, O. Arancio, Rodent models for Alzheimer's disease drug discovery, Expet Opin. Drug Discov. 10 (2015) 703–711.
[50] Q. Zhu, Z. Wang, Distribution characteristics and source analysis of heavy metals in sediments of the main river systems in China, Earth Environ. 40 (2012) 305–313.
[51] K. Borst, A.A. Dumas, M. Prinz, Microglia: immune and non-immune functions, Immunity 54 (2021) 2194–2208.
[52] G.C. Brown, A. Vilalta, How microglia kill neurons, Brain Res. 1628 (2015) 288–297.
[53] K.L. Kumawat, D.K. Kaushik, P. Goswami, A. Basu, Acute exposure to lead acetate activates microglia and induces subsequent bystander neuronal death via caspase-3 activation, Neurotoxicology 41 (2014) 143–153.
[54] Y. Cai, J. Liu, B. Wang, M. Sun, H. Yang, Microglia in the neuroinflammatory pathogenesis of Alzheimer's disease and related therapeutic targets, Front. Immunol. 13 (2022), 856376.
[55] F. Leng, P. Edison, Neuroinflammation and microglial activation in Alzheimer disease: where do we go from here? 17 (2021) 157–172.
[56] J. Kardos, L. Héja, Á. Simon, I. Jablonkai, R. Kovács, K. Jemnitz, Copper signalling: causes and consequences, Cell Commun. Signal. 16 (2018) 1–22.
[57] S. Lutsenko, Dynamic and cell-specific transport networks for intracellular copper ions, J. Cell Sci. 134 (2021), jcs240523.
[58] M.-H. Wen, X. Xie, P.-S. Huang, K. Yang, T.-Y. Chen, Crossroads between membrane trafficking machinery and copper homeostasis in the nerve system, Open Biology 11 (2021), 210128.
[59] S. Montes, S. Rivera-Mancia, A. Diaz-Ruiz, L. Tristan-Lopez, C. Rios, Copper and Copper Proteins in Parkinson's Disease. Oxidative Medicine and Cellular Longevity, 2014, 2014.
[60] S.L. Sensi, A. Granzotto, M. Siotto, R. Squitti, Copper and zinc dysregulation in Alzheimer's disease, Trends Pharmacol. Sci. 39 (2018) 1049–1063.
[61] M. Bisaglia, L. Bubacco, Copper ions and Parkinson's disease: why is homeostasis so relevant? Biomolecules 10 (2020).
[62] I.S. Song, H.H. Chen, I. Aiba, A. Hossain, Z.D. Liang, L.W. Klomp, et al., Transcription factor Sp1 plays an important role in the regulation of copper homeostasis in mammalian cells, Mol. Pharmacol. 74 (2008) 705–713.
[63] Q. Gao, Z. Dai, S. Zhang, Y. Fang, K.K.L. Yung, P.K. Lo, et al., Interaction of Sp1 and APP promoter elucidates a mechanism for Pb2+ caused neurodegeneration, Arch. Biochem. Biophys. 681 (2020), 108265.
[64] A. Tapias, D. Lázaro, B.-K. Yin, S.M.M. Rasa, A. Krepelova, E. Kelmer Sacramento, et al., HAT cofactor TRRAP modulates microtubule dynamics via SP1 signaling to prevent neurodegeneration, Elife 10 (2021), e61531.
[65] K. Bandeen-Roche, T.A. Glass, K.I. Bolla, A.C. Todd, B.S. Schwartz, Cumulative lead dose and cognitive function in older adults, Epidemiology 20 (2009) 831–839.
[66] P.P. Devóz, W.R. Gomes, M.L. De Araújo, D.L. Ribeiro, T. Pedron, L.M. Greggi Antunes, et al., Lead (Pb) exposure induces disturbances in epigenetic status in workers exposed to this metal, J. Toxicol. Environ. Health, Part A 80 (2017) 1098–1105.
[67] S. Solier, S. Müller, A druggable copper-signalling pathway that drives inflammation 617 (2023) 386–394.
[68] M. Vanišová, D. Burská, J. Křížová, T. Daňhelovská, Ž. Dosoudilová, J. Zeman, et al., Stable COX17 downregulation leads to alterations in mitochondrial ultrastructure, decreased copper content and impaired cytochrome c oxidase biogenesis in HEK293 cells, Folia Biol. 65 (2019) 181–187.
[69] N. Wiedemann, N. Pfanner, Mitochondrial machineries for protein import and assembly, Annu. Rev. Biochem. 86 (2017) 685–714.
[70] C. Reinhardt, G. Arena, K. Nedara, R. Edwards, C. Brenner, K. Tokatlidis, et al., AIF meets the CHCHD4/Mia40-dependent mitochondrial import pathway, Biochim. Biophys. Acta, Mol. Basis Dis. 1866 (2020), 165746.
[71] J.R. Inigo, D. Chandra, The mitochondrial unfolded protein response (UPRmt): shielding against toxicity to mitochondria in cancer, J. Hematol. Oncol. 15 (2022) 98.
[72] X. Han, T. Xu, Q. Fang, H. Zhang, L. Yue, G. Hu, et al., Quercetin hinders microglial activation to alleviate neurotoxicity via the interplay between NLRP3 inflammasome and mitophagy, Redox Biol. 44 (2021), 102010.
[73] J. Wu, M.R. Basha, B. Brock, D.P. Cox, F. Cardozo-Pelaez, C.A. McPherson, et al., Alzheimer's disease (AD)-like pathology in aged monkeys after infantile exposure to environmental metal lead (Pb): evidence for a developmental origin and environmental link for AD, J. Neurosci. 28 (2008) 3–9.
[74] D.K. Lahiri, B. Maloney, N.H. Zawia, The LEARn model: an epigenetic explanation for idiopathic neurobiological diseases, Mol. Psychiatr. 14 (2009) 992–1003.
[75] B. Maloney, D.K. Lahiri, Epigenetics of dementia: understanding the disease as a transformation rather than a state, Lancet Neurol. 15 (2016) 760–774.